Shape coexistence and multiparticle-multihole structures in ^{110,112}Cd

P. E. Garrett *et al.*

Phys. Rev. C **101**, 044302 — Published 9 April 2020

DOI: 10.1103/PhysRevC.101.044302

Shape coexistence and multiparticle-multihole structures in ^{110,112}Cd

P.E. Garrett,[1,2] T.R. Rodríguez,[3] A. Diaz Varela,[1] K.L. Green,[1] J. Bangay,[1] A. Finlay,[1] R.A.E. Austin,[4] G.C. Ball,[5] D.S. Bandyopadhyay,[1] V. Bildstein,[1] S. Colosimo,[4] D.S. Cross,[6] G.A. Demand,[1] P. Finlay,[1] A.B. Garnsworthy,[5] G.F. Grinyer,[7] G. Hackman,[5] B. Jigmeddorj,[1] J. Jolie,[8] W.D. Kulp,[9] K.G. Leach,[1,*] A.C. Morton,[5,†] J.N. Orce,[2] C.J. Pearson,[5] A.A. Phillips,[1] A.J. Radich,[1] E.T. Rand,[1,‡] M.A. Schumaker,[1] C.E. Svensson,[1] C. Sumithrarachchi,[1,†] S. Triambak,[2] N. Warr,[8] J. Wong,[1] J.L. Wood,[10] and S.W. Yates[11]

[1]*Department of Physics, University of Guelph, Guelph, ON, N1G2W1 Canada*
[2]*Department of Physics and Astronomy, University of the Western Cape, P/B X17, Bellville ZA-7535, South Africa*
[3]*Departamento de Física Teórica and CIAFF, Universidad Autónoma de Madrid, E-28049 Madrid, Spain*
[4]*Department of Physics and Astronomy, St. Mary's University, Halifax, NS, Canada*
[5]*TRIUMF, 4004 Wesbrook Mall, Vancouver, BC, V6T2A3 Canada*
[6]*Department of Chemistry, Simon Fraser University, Burnaby, BC, Canada*
[7]*Department of Physics, University of Regina, Regina, SK S4S0A2, Canada*
[8]*Institut für Kernphysik, Universität zu Köln, Zülpicherstrasse 77, D-50937 Köln, Germany*
[9]*Defense Threat Reduction Agency, 8725 John J Kingman Rd, Ft. Belvoir, VA 22060-6217 USA*
[10]*Department of Physics, Georgia Institute of Technology, Atlanta, GA, USA*
[11]*Departments of Chemistry and Physics & Astronomy, University of Kentucky, Lexington, KY, 40506-0055 USA*

From detailed spectroscopy of ^{110}Cd and ^{112}Cd following the β^+/EC decay of ^{110,112}In and the β^- decay of ^{112}Ag, the presence of very weak decay branches from non-yrast states is revealed. In ^{112}Cd, $2^+_5 \rightarrow 0^+_4$ and $4^+_6 \rightarrow 2^+_5$ transitions are observed that yield $B(E2; 2^+_5 \rightarrow 0^+_4) = 34 \pm 15$ W.u. and $B(E2; 4^+_6 \rightarrow 2^+_5) = 77 \pm 30$ W.u., respectively, clearly indicating a collective structure. In ^{110}Cd, a weak decay branch from the 4^+_6 level to the 2^+_5 level is observed, and from a lifetime measurement following the $(n, n'\gamma)$ reaction, the $B(E2; 4^+_6 \rightarrow 2^+_5) = 55 \pm 14$ W.u. is determined. A new branch is also observed for the decay of the 6^+_4 level to the 4^+_6 state, indicating that the sequence 2^+_5, 4^+_6, and 6^+_4 forms part of a collective structure. The presence of 3^+_3 and 5^+_2 levels spaced between the previous sequence is highly suggestive of a γ-band built on the 0^+_2 shape-coexisting intruder state. The 0^+_4 levels in ^{110,112,114}Cd have preferred decays to the lowest 2^+ members of the intruder bands, and for ^{114}Cd a previous measurement had established an enhanced $B(E2; 0^+_4 \rightarrow 2^+_3)$. The energy systematics of the 0^+_2, 0^+_3, and 0^+_4 levels all display the characteristic parabolic-shaped pattern suggesting that they are built on multiparticle-multihole proton excitations. The results are compared with beyond-mean-field calculations that reproduce qualitatively the observed levels and their decays, and suggest that the 0^+_1, 0^+_2, 0^+_3, and 0^+_4 levels, and the excited states built on them, possess different deformations.

PACS numbers: 21.10.Re,21.60.Ev,23.20.Lv,23.40.Hc

I. INTRODUCTION

In regions near magic nuclei, the mechanism behind shape coexistence is often described as the promotion of pairs of particles across the closed shells that leads to enhancements in the correlation energy in the system, thereby offsetting the energy required to promote a pair of particles. The correlation energy increases with the number of particles involved in such interactions and, largely driven by the proton-neutron interaction, can give rise to the characteristic parabolic-shaped pattern of the excitation energy of the multiparticle-multihole states as a function of the particle number, reaching a minimum near the middle of the shell. This pattern has been observed in many isotopic chains, with the classic examples being the Cd/Sn isotopes (see Ref. [1] for a recent review) and the Hg/Pb isotopes (see, e.g., Ref. [2] and references therein).

In lighter nuclei, shape coexisting states based on multiparticle-multihole configurations have been identified and firmly established. For example, in ^{40}Ca, the $0p0h$ spherical ground state coexists with $\pi(2p2h) \otimes \nu(2p2h)$ and $\pi(4p4h) \otimes \nu(4p4h)$ states [3], the band structures for which have been identified [4]. Recently, detailed Coulomb excitation measurements [5, 6] have established firmly the highly deformed shapes of the $6p4h$ structures in ^{42}Ca. In heavier nuclei, such examples of coexisting multiparticle-multihole configurations at low-spin have not been firmly established. Such configurations should exist, but identifying them has proven to be challenging. To date, some of the best evidence for such configurations has been obtained in the Pb region [7]. Another rarity in shape-coexistence regions is evi-

* Present address: Department of Physics, Colorado School of Mines, 1523 Illinois St., Golden, CO 80401, USA
† Present address: National Superconducting Cyclotron Center, Michigan State University, East Lansing, MI 48824, USA
‡ Present address: Applied Physics Branch, Canadian Nuclear Laboratories, 286 Plant Road, Chalk River, ON K0J 1J0, Canada

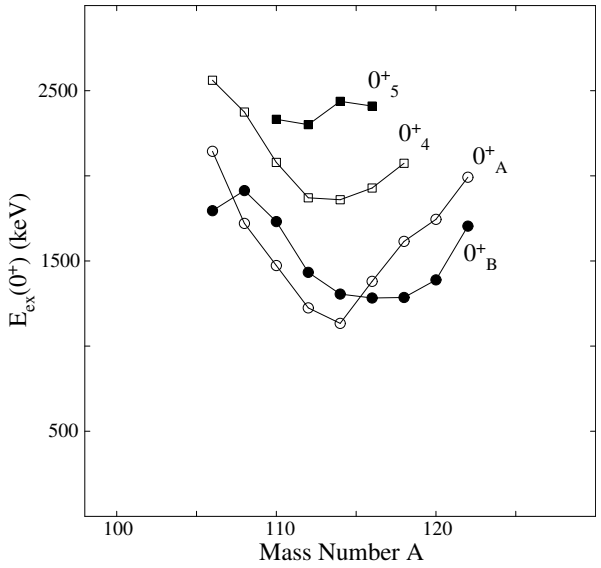

FIG. 1. Observed excitation energies of 0^+ states in the even-even Cd isotopes. The excited 0^+ states labeled 0^+_A have been assigned as the heads of shape coexisting band based on a $\pi(2p4h)$ configuration. The close-lying 0^+_B levels have been previously interpreted as two-phonon vibrational states that underwent mixing with the intruder states, and the 0^+_4 levels were assigned as three-phonon states. The 0^+_5 states may represent a predominately two-quasiparticle configuration; in ^{110,112}Cd they receive moderate population in single-neutron-transfer reactions [23, 31, 40].

dence for multiple shapes at low excitation energy. While the presence of multiparticle-multihole excitations is suggestive of different shapes, and these are supported by theoretical calculations, firmly establishing the nature of observed sequences of states (or bands) is often hampered by their location. For example, even in one of the most cited examples of multiple shapes, ^{186}Pb [8], the evidence for the presence of different shapes is circumstantial, largely due to the fact that this nucleus is far from stability and hence difficult to study. In the present work, which expands on the details given in Ref. [9], evidence is presented suggesting that ^{110,112}Cd have low-lying 0^+ states that possess different shapes.

The presence of shape-coexisting $\pi(2p4h)$ bands in Cd nuclei, hereafter referred to as the intruder bands, was first suggested in Refs. [10, 11] and experimentally established in ^{110}Cd in Ref. [12], and was investigated through the use of the Pd($^3He, n$) two-proton transfer reactions [13]. In these reactions, strongly enhanced cross sections for the 0^+_2 states in ^{110,112}Cd, consistent with the assigned $\pi(2p4h)$ nature assuming the Pd target ground states are $\pi 4h$, were observed. Systematic studies, employing a wide variety of reactions and techniques [14–48] focused largely on the vibrational multiphonon states and the shape-coexisting intruder bands in the even-even Cd isotopes. It was noted in Ref. [49] that the 0^+_4 level had the characteristics of an intruder excitation, and it

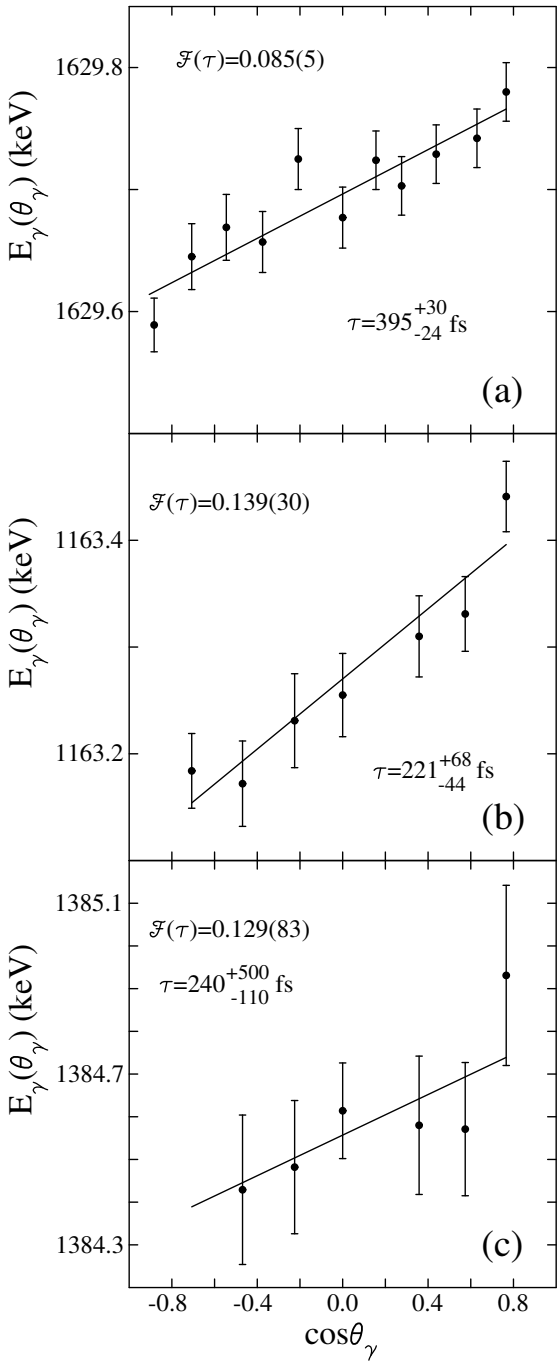

FIG. 2. Observed γ-ray energies from the ^{110}Cd($n, n'\gamma$) reaction as a function of the $\cos\theta_\gamma$ for the 1630 keV γ ray from the 2288 keV 2^+ level (a), the 1163 keV γ ray from the 2706 keV 4^+ level (b), and the 1385 keV γ ray from the 2927 keV 5^+ state (c). $\mathcal{F}(\tau)$ values and the deduced level lifetimes are shown.

was further speculated in Ref. [28] that the 0^+_4 state in ^{110}Cd could be the $\pi(4p6h)$ state, and may possess a higher degree of deformation. In the present work, this suggestion is generalized, with the aid of beyond-mean-

field calculations, to the possibility of that there exists multiple-shape coexistence in the mid-shell Cd isotopes ^{110,112}Cd. This suggestion provides an alternative view of the Cd isotopes in contrast to their long-held standing as some of the best examples of nearly harmonic vibrational motion. We hope that the present work will spur additional studies, both experimental and theoretical, to firmly establish the nature of the states and to provide a framework for their understanding.

II. EXPERIMENTAL DETAILS AND RESULTS

The results presented here combine β-decay measurements that were focused on weak, low-energy transitions, and lifetime determinations from $(n, n'\gamma)$ reactions. The β decays of ^{110}In and ^{112}In/^{112}Ag were studied using the 8π spectrometer [50, 51] at the TRIUMF-ISAC facility [52]. For the mass 110 decay experiment, a 65 μA, 500 MeV proton beam was directed onto a ^{nat}Ta production target. The reaction products that diffused to the surface of target foils were ionized with a Re surface-ionization source and passed through a magnetic mass separator set to select singly charged $A = 110$ ions. The resultant beam delivered to the 8π spectrometer consisted of 1.2×10^7 s^{-1} of ^{110}In^g ($I^\pi = 7^+$, $t_{1/2} = 4.9$ h) and 1.7×10^6 s^{-1} of ^{110}In^m ($I^\pi = 2^+$ $t_{1/2} = 1.15$ h). Selected results from this experiment that focused on the decays of the purported vibrational multiphonon levels and the intruder band were published earlier [28]. For the mass 112 decay measurement, a 40 μA 500-MeV proton primary beam was used, and the Ag reaction products were ionized using TRILIS [53]. The extracted and mass-separated radioactive beam included 7.5×10^6 s^{-1} of ^{112}In^m ($t_{1/2} = 20.6$ min, $I^\pi = 7^+$), 2.3×10^6 s^{-1} of ^{112}In^{gs} ($t_{1/2} = 15$ min, $I^\pi = 1^+$), and 4.8×10^5 s^{-1} of ^{112}Ag ($t_{1/2} = 3.1$ h, $I^\pi = 2^{(-)}$).

Each beam was deposited onto an FeO-coated mylar tape at the center of the 8π spectrometer, which consisted of 20 high-purity Ge (HPGe) detectors with bismuth germanate (BGO) Compton-suppression shields. The average source-to-Ge-detector distance was 14 cm. A BC-422Q fast plastic scintillator with a solid angle of approximately 20% was located immediately behind the beam deposition point, while the 5 Si(Li) detectors of the PACES array for high-resolution conversion-electron studies were positioned upstream. The data were collected in scaled-down γ singles, γ-γ coincidences, scaled-down Si singles, and γ-Si coincidence modes. Cycling of the beam deposition and tape movement was employed to emphasize the decays of interest. For the ^{110}In decay measurement, the cycles consisted of approximately 1 h of beam deposition plus 1 h of decay, after which the source position on the tape was moved to a point outside the array behind a lead wall and the cycle repeated. For the mass 112 decay measurements, the decays of interest were those associated with ^{112}Ag, and thus a source was produced during an approximately 9-hour beam deposition, allowed to cool for approximately 1 to 2 hours to reduce the In activities, and then counted for a period of 6 to 8 hours. This beam-on, beam-off cycling allowed for a more sensitive study than that reported in Ref. [38] since the In activity was greatly reduced.

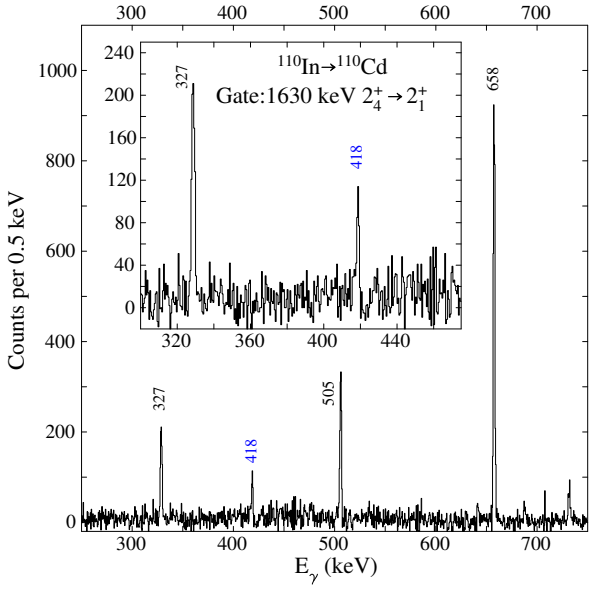

FIG. 3. Portion of the spectrum of γ rays in coincidence with the 1630 keV $2_4^+ \rightarrow 2_1^+$ γ ray in ^{110}Cd. The 418 keV γ ray is assigned as the 2706 keV $4_5^+ \rightarrow$ 2288 keV 2_4^+ transition. The spectrum inset shows the detail near the 418 keV γ-ray peak.

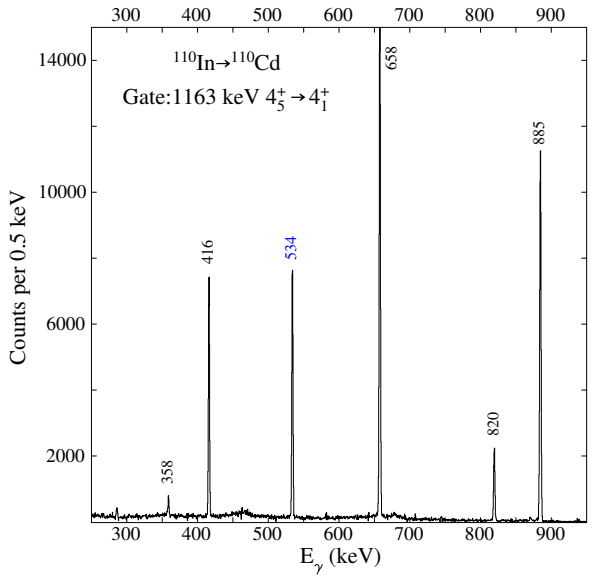

FIG. 4. Portion of the spectrum of γ rays in coincidence with the 1163 keV $4_5^+ \rightarrow 4_1^+$ γ ray in ^{110}Cd. The 534 keV γ ray is assigned as the 3240 keV $6_5^+ \rightarrow$ 2706 keV 4_5^+ transition.

Branching ratios were generally determined by using

the gating from below technique [54] where

$$N_{12} = \mathcal{N} I_{\gamma_1} \epsilon(\gamma_1) B_{\gamma_2} \epsilon(\gamma_2) \epsilon_C \eta(\theta_{12}) \quad (1)$$

with N_{12} the number of counts in the coincidence peak between two cascading γ rays, I_{γ_1} is the intensity of the "feeding" γ ray of the pair, B_{γ_2} is the branching fraction of the "draining" transition γ_2, and $\epsilon(\gamma)$ the detection efficiency at energy E_γ. The factor $\mathcal{N}$ is an overall normalization constant that characterizes a given decay data set, ϵ_C reflects the change in the detection efficiency due to the coincidence condition, and $\eta(\theta_{12})$ is the effect of the angular correlation. For the present data, the assumption is made that the time conditions applied during the sorting of the data did not distort the detection efficiency, and corrections due to angular correlations and summing effects are in general below $\pm 3\%$ due to the symmetry of the 8π spectrometer resulting from the icosahedral positioning of the γ-ray detectors [54]. Relabeling $I'_{\gamma_1} = N_{12}/\epsilon(\gamma_1)$, the branching ratio for any level can be found from

$$BR(\gamma_1) = \frac{\dfrac{I'_{\gamma_1}}{B_{\gamma_2}\epsilon(\gamma_2)}}{\displaystyle\sum_j \frac{I'_{\gamma_{1j}}}{B_{\gamma_{2j}}\epsilon(\gamma_{2j})}} \quad (2)$$

where the summation over j extends to all transitions decaying from the level of interest. Detailed tests of the procedure, and the equivalence of the results from gating from below *vs.* gating from above, are given in Ref. [55].

The branching ratios determined from the β-decay results have been combined with the lifetimes resulting from the $(n, n'\gamma)$ studies published in Ref. [28] or newly determined herein, from a re-analysis of a previously obtained data set [26, 27], via the Doppler-shift attenuation method following inelastic neutron scattering. The method and procedures are outlined in Ref. [56]. Briefly, nearly monoenergetic neutrons were produced via the ^{3}H$(p, n)^3$He reaction at he University of Kentucky accelerator facility. Angular distributions were obtained from recording the γ-ray spectra, using a Compton-suppressed HPGe detector with approximately 50% relative efficiency located ≈ 1.1 m from the CdO scattering sample, at angles varying from $\theta_\gamma = 40°$ to $152°$ with respect to the proton beam axis. The observed γ-ray energy is

$$E_\gamma(\theta_\gamma) \approx E^0_\gamma \left(1 + \beta \mathcal{F}(\tau) \cos\theta_\gamma\right) \quad (3)$$

where E^0_γ is the unshifted γ-ray energy, β is the recoil velocity in the center of mass frame, and $\mathcal{F}(\tau)$ is the attenuation factor derived from a modeling of the slowing-down process of the Cd recoiling nuclei in the CdO medium, based on the formalism in Ref. [56]. Figure 2 displays the Doppler shifts of the most intense decay γ rays from the 2288 keV level (1630 keV γ ray), the 2706 keV state (1163 keV), and the 2927 keV level (1385 keV). From the fits to the Doppler shifts, and comparisons with calculations for the $\mathcal{F}(\tau)$ values, lifetimes for the 2288, 2706, and 2927 keV levels of $\tau = 395^{+30}_{-24}$, $\tau = 221^{+68}_{-44}$, and $\tau = 240^{+500}_{-110}$ fs were determined.

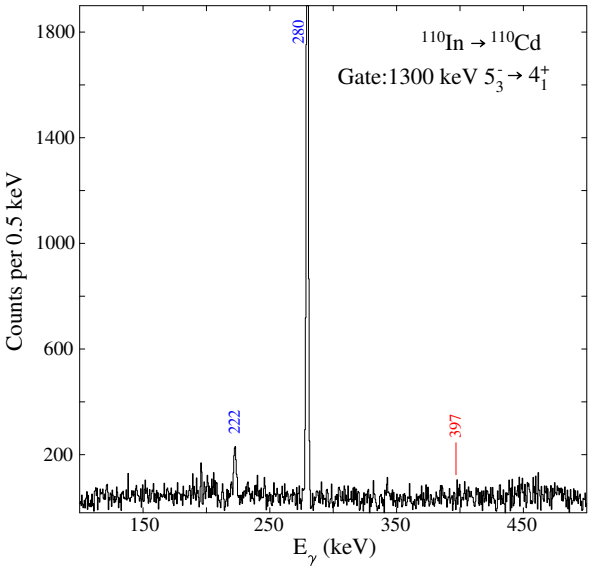

FIG. 6. Portion of the spectrum of γ rays in coincidence with the 1300 keV $5^-_3 \rightarrow 4^+_1$ γ ray in ^{110}Cd. The newly observed γ rays of 222 keV from the 3064 keV 6^+ level, and 280 keV from the 3121 keV 6^+ level are labeled. The position of a previously assigned [22] 397 keV γ ray from the 3240 keV 6^+ level is indicated.

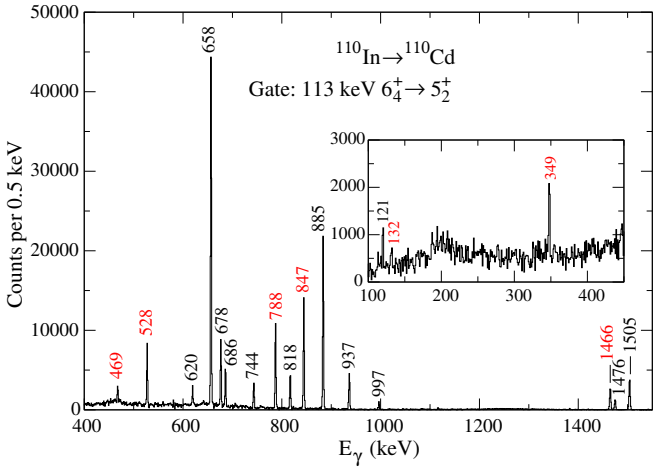

FIG. 5. Portion of the spectrum of γ rays in coincidence with the 113 keV $6^+_4 \rightarrow 5^+_2$ γ ray in ^{110}Cd. The energies of the observed decays of the 3008 keV 5^+ state are labeled in red (light gray).

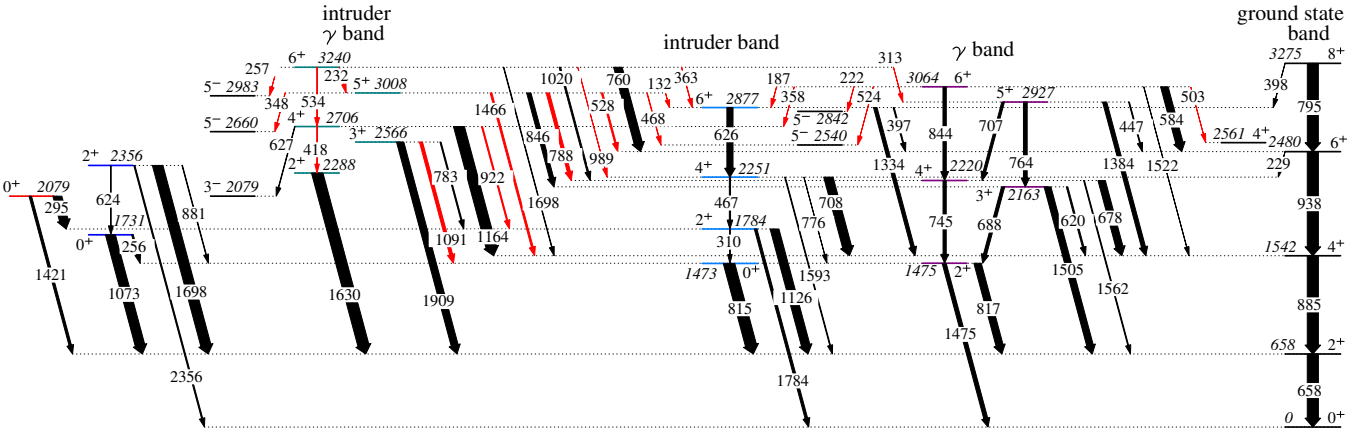

FIG. 7. Partial level scheme of ^{110}Cd. The widths of the arrows are proportional to the measured branching values, and transitions are labeled with their energies in keV. Newly observed transitions are colored red (light gray). The levels are organized in sequences of rotational-like bands. The traditional labels for the bands as 'intruder' and 'γ' are used, irrespective of the precise nature of the underlying configuration.

A. Spectroscopy of ^{110}Cd

In ^{110}Cd, the decay of the 0_4^+ level favoring the feeding of the 1783 keV 2^+ intruder band member was confirmed in Ref. [28]. We have sought evidence for higher-lying 2^+ states feeding the 0_4^+ level, but none could be firmly identified. The further analysis of weak decay branches, however, has revealed a new transition feeding the 2_4^+ level at 2288 keV. Figure 3 displays a partial spectrum of γ rays in coincidence with the 1630 keV $2_4^+ \rightarrow 2_1^+$ γ ray, where the presence of a 418 keV γ ray can clearly be seen. This γ ray is assigned as the 2706 keV $\rightarrow$ 2288 keV 2_4^+ transition. The branching ratio for this transition, 0.59(5)%, is determined using the gating from below method.

Figure 4 shows the part of the spectrum of γ rays in coincidence with the 1163 keV γ ray – the largest decay branch from the 2706 keV state. The 534 keV γ ray, assigned as feeding the 2706 keV level, is due to a decay from the 3240 keV 6^+ state. The 2706 keV level was previously suggested to be 4^- by Kern *et al.* [22], but 4^+ by Corminboeuf *et al.* [27], leading to ambiguity in its parity. The presence of the 534 keV γ-ray decay from the 6^+ state feeding the 2706 keV level, and its decay by a 418 keV γ ray to the 2287 keV 2^+ level leads to a firm assignment of 4^+.

A new level at 3008 keV was established by Jigmeddorj *et al.* [57], and assigned as 5^+ based on the observed decay to the 2163 keV 3^+ level, and its feeding by a 113 keV transition of mixed $E2/M1$ nature from the 3122 keV 6^+ level. Figure 5 displays the spectrum of γ rays in coincidence with the 113 keV γ ray feeding the 3008 keV state, and shows the presence of 7 de-exciting transitions.

The 3240 keV level was observed previously in the β-decay of ^{110}In [58], as well as with the ^{108}Pd$(\alpha, 2n\gamma)$ reaction [22], and was assigned as 6^+. In the study by Kern *et al.* [22], a 397 keV γ ray was placed as de-exciting this level and feeding the 2842 keV 5^- state; however, it was noted that it was possibly a doublet, and that its placement was questionable. Figure 6 displays the γ rays in coincidence with the 1300 keV $5_3^- \rightarrow 4_1^+$ γ ray, where the presence of the newly observed 222 keV $6_3^+ \rightarrow 5_3^-$ peak and the absence of the 397 keV peak are apparent.

Figure 7 displays a partial level scheme for ^{110}Cd showing the decay γ rays observed. The newly observed transitions are indicated, and the levels are organized into sequences as proposed in Ref. [9] and are labeled as the ground-state band, the intruder band for the $\Delta I = 2$ sequence built on the 0_2^+ level, the γ band for the $\Delta I = 1$ sequence built on the 2_2^+ state, and the intruder γ band for the $\Delta I = 1$ sequence built on the 2_4^+ state at 2288 keV. (We use the traditional nomenclature "intruder" and "γ" as labels for these excitations, independent of their precise natures.) Table I lists the results for the transitions displayed in Fig. 7 that have not been reported previously [28], and includes the new lifetime information.

In the cases where the levels are connected by enhanced $E2$ transitions, assigning them as part of a band sequence is rather straightforward. This procedure is largely the case for the ground-state band, the γ band based on the 1475 keV level, and the intruder band based on the 1473 keV level. The 2706 keV 4^+ state and 3240 keV 6^+ state have decays with enhanced $B(E2)$ values to the 2288 keV 2^+ and 2706 keV 4^+ states, respectively, strongly indicating that they also form part of a collective structure. However, these states could be assigned as part of a 0^+ band, built on the 2079 keV 0^+ state, or another "$K = 2$" band. The latter assignment is favored due to the presence of the 3^+ and 5^+ states at 2566 and 3008 keV. While there are other 3^+ states in the vicinity, specifically at 2433 keV and 2662 keV, these were strongly populated in the ^{111}Cd(d, t) reaction [23] and are thus assigned as hav-

TABLE I. New results for the levels in ^{110}Cd displayed in Fig. 7. The 1σ uncertainties are indicated in parentheses, and quantities surrounded by square brackets in the final column are relative $B(E2)$ values.

E_i (keV)	I_i^π	E_γ (keV)	E_f	I_f^π	Branching	δ	$F(\tau)$, τ (fs)	$B(E2; I_i \to I_f)$
2079.2	0_4^+	295.66(12)	1783.2	2_3^+	0.783(45)			[100(3)]
		1421.80(21)	657.8	2_1^+	0.217(45)			[0.011(1)]
2287.5	2_4^+	1629.711(10)[a]	657.8	2_1^+	1	2.22^{+19}_{-18}, 0.020^{+27}_{-36}	0.085(5), 395^{+30}_{-24}	4.78(35), 0.0023(9)
2566.5	3_3^+	782.937(14)[a]	1783.6	2_3^+	0.097(1)	$-25^{+12}_{-\infty}$, 0.15(4)	0.044(8), 770^{+180}_{-120}	11(2), 0.25^{+12}_{-15}
		1090.654(7)[a]	1475.8	2_2^+	0.269(3)	0.33(3)		0.59(14)
		1908.665(7)[a]	657.8	2_1^+	0.634(3)	0.20(2)		0.032(10)
2705.7	4_5^+	418.05(13)	2287.3	2_4^+	0.0059(5)		0.139(30), 221^{+68}_{-44}	55(14)
		626.82(14)	2078.6	3_1^-	0.0412(88)			
		921.93(12)	1783.6	2_3^+	0.0031(3)			1.3(4)
		1163.31(12)[a]	1542.5	4_1^+	0.9500(88)	1.18^{+20}_{-18}, $-0.04(7)$		31(9), 0.09^{+56}_{-9}
2876.4	6_2^+	397.05(11)	2479.8	6_1^+	0.0920(34)			[< 164(36)]
		626.19(11)	2250.2	4_3^+	0.549(10)			[100(1)]
		1334.38(11)	1542.3	4_1^+	0.310(9)			[1.29(1)]
2926.7	5_1^+	446.85(12)	2479.8	6_1^+	0.0741(25)		0.129(83), 240^{+500}_{-110}	$< 58^{+46}_{-39}$
		706.67(12)	2219.8	4_3^+	0.228(7)			$< 78^{+62}_{-52}$
		763.924(31)[a]	2162.6	3_1^+	0.334(8)			140^{+110}_{-90}
		1384.557(65)[a]	1542.4	4_1^+	0.365(9)			$< 7^{+6}_{-5}$
3008.1	5_2^+	131.92(6)	2876.4	6_2^+	0.0029(2)			[< 8400(600)]
		348.57(20)	2659.8	5_2^-	0.0193(5)			
		468.62(16)	2539.5	5_1^-	0.0401(8)			
		528.39(8)	2479.8	6_1^+	0.1290(16)			[< 363(5)]
		788.29(6)	2219.8	4_3^+	0.2823(26)			[< 107(1)]
		845.54(6)	2162.6	3_1^+	0.3729(29)			[100(1)]
		1465.88(13)	1542.3	4_1^+	0.1536(20)			[< 2.63(3)]
3063.9	6_3^+	187.53(12)	2876.4	6_2^+	0.0191(4)	< 1.3[b]		[< 7500(160)]
		221.87(12)	2842.3	5_3^-	0.00023(1)			
		358.57(12)	2705.6	4_5^+	0.00070(2)			[17.1(5)]
		502.86(13)	2561.2	4_4^+	0.00093(5)			[4.2(2)]
		524.50(12)	2539.5	5_1^-	0.0056(1)			
		584.17(11)	2479.8	6_1^+	0.6584(58)	0.0(3)[c]		[< 115(1)]
		844.09(11)	2219.8	4_3^+	0.2966(53)			[100(2)]
		1521.75(12)	1542.3	4_1^+	0.0184(4)			[0.32(1)]
3239.6	6_4^+	231.54(14)	3008.1	5_2^+	0.00195(15)			[< 420(20)]
		255.78(14)	2983.8	5_4^-	0.00018(1)			
		313.31(12)	2926.4	5_2^+	0.0041(2)			[< 200(5)]
		363.19(12)	2876.4	6_2^+	0.0290(13)			[< 670(12)]
		534.08(12)	2705.6	4_5^+	0.0297(12)			[100(2)]
		759.91(12)	2479.8	6_1^+	0.745(7)	$-0.29(10)$[c]		$[33^{+24}_{-19}]$
		989.37(12)	2250.2	4_3^+	0.0125(8)			[1.9(1)]
		1019.77(12)	2219.8	4_2^+	0.133(5)			[17.7(3)]
		1697.42(12)	1542.3	4_1^+	0.0465(19)			[0.48(1)]

[a] γ-ray energy determined from the $(n, n'\gamma)$ results.
[b] Value deduced from α_K values published in Ref. [57].
[c] Value taken from Ref. [22].

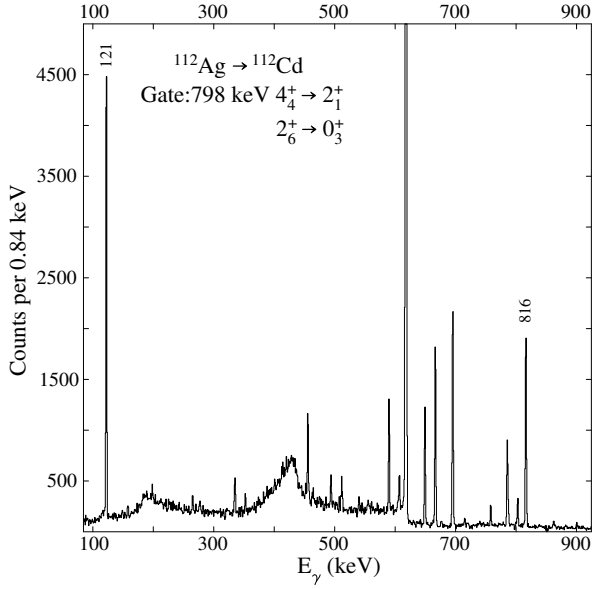

FIG. 8. Portion of the spectrum of γ rays in coincidence with the 798 keV doublet of γ rays. The γ rays at 121 and 816 keV originate from the 1433 keV 0_3^+ level, and establish the existence of the 798 keV transition from the 2231 keV 2^+ state (nearly all of the remaining unlabeled peaks in the spectrum are in coincidence with the 798 keV $4_1^+ \rightarrow 2_1^+$ γ ray).

ing predominately two-quasiparticle character with configurations $\nu s_{1/2} d_{5/2}$ and $\nu s_{1/2} g_{7/2}$, respectively. (The 2561 keV 4^+ state is also assigned as the $\nu s_{1/2} g_{7/2}$ configuration based on its strong population in the ^{111}Cd(d,t) reaction [23].) The 2566 keV state, on the other hand, possesses an enhanced $E2$ decay to the 2^+ member of the intruder band, with $B(E2; 3_3^+ \rightarrow 2_3^+) = 11(2)$ W.u. (using the favored value for the mixing ratio). The presence of the 3^+ and 5^+ states thus completes the sequence of levels expected for an excited γ band. This $\Delta J = 1$ sequence is labeled as the "intruder γ-band". Unfortunately, the 0^+ band based on the 1731 keV level could not be extended beyond spin 2, and no members could be assigned to the 2079 keV 0^+ band at the present time. In both cases there are higher-lying candidates, but the absence of any observed inband transitions prevents firm assignments.

B. Spectroscopy of ^{112}Cd

The decay of ^{112}Ag ($t_{1/2} = 3.1$ h, $2^{(-)}$) populates low-spin states in ^{112}Cd, facilitating the investigation of γ-ray decays of spin 0–2 states, especially. Figure 8 shows a portion of the spectrum of γ rays in coincidence with the 798 keV γ ray. This particular γ ray is assigned as the $4_1^+ \rightarrow 2_1^+$ transition in ^{112}Cd, but the spectrum in Fig. 8 shows clearly the presence of the 121 and 816 keV γ rays, which are known to be the depopulating γ rays from the 1433 keV 0_3^+ level, as displayed in Fig. 9 where the bands are labeled analogously to those in Fig. 7. The presence of these γ rays in the coincidence spectrum clearly implies the existence of a 798 keV γ ray feeding the 1433 keV 0^+ state from the 2231 keV 2_6^+ level. From the data presented in Fig. 8, branchings for the decays from the 1433 keV 0_3^+ level were determined and are listed in Table II.

Using data from an experiment to study the decay of ^{112}Ag performed earlier at TRIUMF-ISAC, the decay of the 1871 keV 0_4^+ level was clarified [38]. Shown in Fig. 10 is a portion of the spectrum of γ rays in coincidence with the 636 keV $1_1^- \rightarrow 0_4^+$ γ ray in ^{112}Cd obtained from the present data. The two γ rays assigned to the decay of the 0_4^+ level, the 403 keV $0_4^+ \rightarrow 2_3^+$ γ ray, and the 1254 keV $0_4^+ \rightarrow 2_1^+$ γ ray, are observed with higher statistics than before [38], and thus higher precision for the branching ratio is achieved.

Additionally, the present data enable possible decays of higher-lying states to the 0_4^+ level to be sought. Figure 11 displays the γ-ray spectrum in coincidence with the 1254 keV γ ray which decays from the 1871 keV 0^+ state. Shown in the inset is the small peak due to the 360 keV γ ray that is assigned as the 2231 keV $2_6^+ \rightarrow 0_4^+$ transition; its branching ratio is determined to be $3.9(4) \times 10^{-4}$ which, using the lifetime of the 2231 keV level from Ref. [37], yields $B(E2; 2_6^+ \rightarrow 0_4^+) = 7.5(15)$ W.u. Far more intriguing, however, is the very small peak from a 285 keV γ ray assigned as the $2_5^+ \rightarrow 0_4^+$ transition. A fit to the peak results in a branching of $7.9(33) \times 10^{-4}$, yielding $B(E2; 2_5^+ \rightarrow 0_4^+) = 34(15)$ W.u., establishing the 2156 keV 2^+ level as the 2^+ band member based on the 1871 keV 0^+ state.

The spin of the ^{112}Ag parent, $2^{(-)}$, does not favor the population of the higher-spin states in ^{112}Cd. Furthermore, the region of the γ-ray spectra where possible $4^+ \rightarrow 2^+$ transitions would be located have a significant amount of Compton background from higher-energy γ rays. Nonetheless, using the knowledge of the locations of the 4^+ excited states, the possible $4^+ \rightarrow 2_5^+$ transitions were sought. Greater sensitivity for observing the transitions was achieved by placing a condition on the γ-γ matrix at the energy of the $4^+ \rightarrow 2^+$ transitions and seeking evidence for the 1539 keV γ ray, as shown in Fig. 12. The spectrum clearly displays the existence of a small peak due to the 1539 keV $2_5^+ \rightarrow 2_1^+$ γ ray. The extracted branching for the 555 keV $4_6^+ \rightarrow 2_5^+$ γ ray is 0.059 ± 0.008, leading to $B(E2; 4_6^+ \rightarrow 2_5^+) = 77 \pm 30$ W.u.

Inspection of the level schemes displayed in Figs. 7 and 9 leads to the conclusion that the excitations in ^{110}Cd and ^{112}Cd are very similar. While in ^{110}Cd the decay scheme is better established for the higher-spin levels, and members of the excited γ band could be suggested, in ^{112}Cd it is the 0^+ bands that are better established.

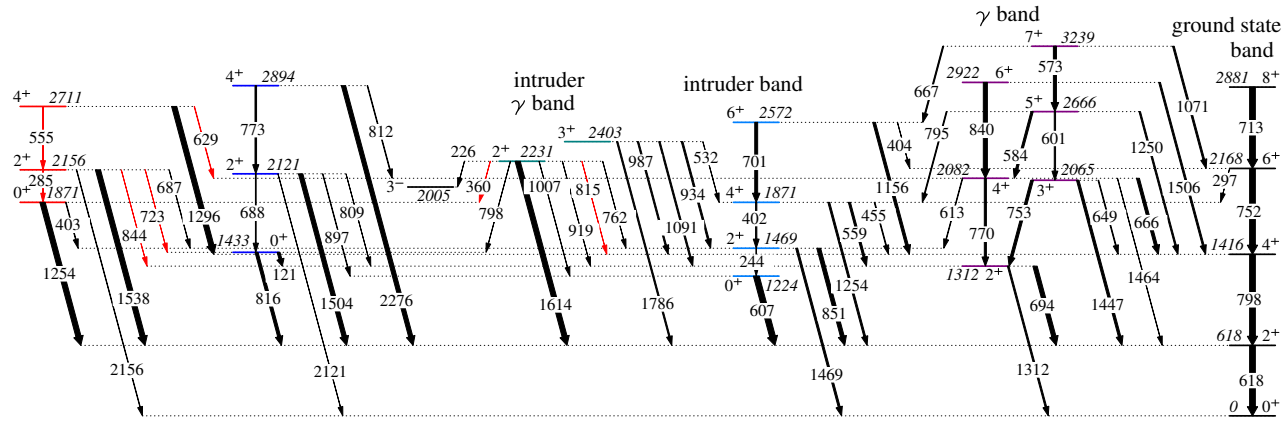

FIG. 9. Partial level scheme of ^{112}Cd. See caption to Fig. 7.

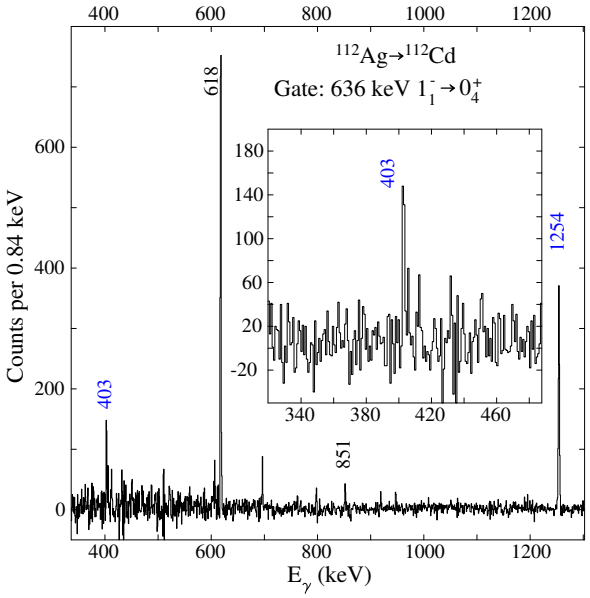

FIG. 10. Portion of the spectrum of γ rays in coincidence with the 636 keV $1_1^- \rightarrow 0_4^+$ γ ray in ^{112}Cd. The peaks are labeled with their energies in keV; the 403 keV and 1254 keV γ rays originate from the decay of the 1871 keV 0_4^+ level. The spectrum inset shows the detail near the 403 keV γ ray, the transition from the 0_4^+ level to the 1469 keV 2^+ member of the intruder band.

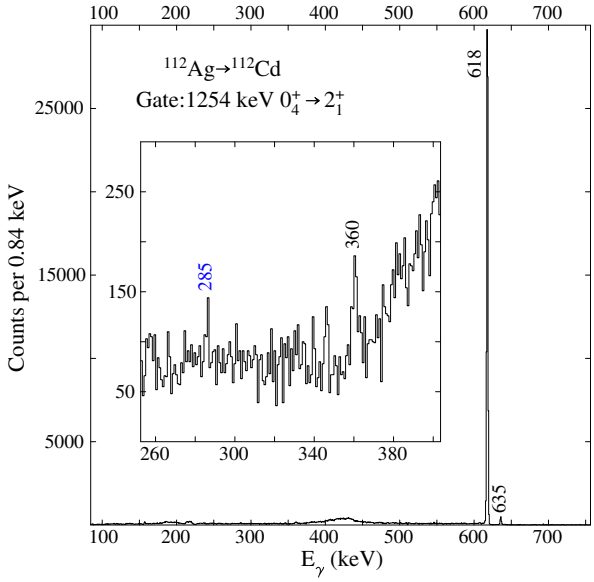

FIG. 11. Portion of the spectrum of γ rays in coincidence with the 1254 keV $0_4^+ \rightarrow 2_1^+$ γ ray. The inset shows the expanded region near 300 keV; the newly observed 285 and 360 keV γ rays are indicated.

III. THEORETICAL CALCULATIONS

As was noted earlier, the behaviors of the 0^+ states in the Cd isotopes are striking. The shape-coexisting intruder band heads, the 0_2^+ states, have enhanced (or possibly enhanced) $E2$ decays to the 2_1^+ levels. The 0_3^+ states have a strongly enhanced decays to the 2_2^+ levels, the γ band heads, and very weak $E2$ decays to the 2_1^+ states. The 0_4^+ levels have strongly preferred decays to the 2^+ members of the intruder bands, rather than the 2^+ members of the ground state bands. These systematic observations are highlighted in Fig. 13, where the branching ratio data from the present work are used to determine the $B(E2)$ values. In ^{114}Cd, the matrix elements for excitation of the 0_4^+ level were determined in a detailed Coulomb excitation experiment [43]; the results of which are consistent with subsequent lifetime measurements [44, 45]. The Coulomb excitation results reveal not only a preferred decay of the 0_4^+ level to the 2^+ member of the intruder band, but also that it is enhanced and of the same order of magnitude as the decay of the 0^+ intruder band head to the 2_1^+ state.

As was outlined above, it was already suggested Ref. [28] that the 0_4^+ states in the Cd nuclei may be based

TABLE II. New results for the levels in ^{112}Cd displayed in Fig. 9. The mixing ratios δ and lifetimes τ are taken from Refs. [36, 37] unless otherwise noted.

E_i (keV)	I_i^π	E_γ (keV)	E_f	I_f^π	Branching	δ	τ	$B(E2; I_i \to I_f)$
1312.4	2_2^+	694.90(11)	617.5	2_1^+	0.734(3)	-4.0(7)[a]	2740(430)[a]	40^{+7}_{-5}
		1312.38(11)	0	0_1^+	0.266(3)			0.64^{+12}_{-9}
1433.4	0_3^+	120.96(12)	1312.4	2_2^+	0.485(11)			78(5)
		815.87(10)	617.5	2_1^+	0.515(11)			0.016(1)
1468.8	2_3^+	244.10(15)	1224.4	0_2^+	0.0090(4)		3900(720)[a]	67^{+15}_{-11}
		851.25(10)	617.5	2_1^+	0.6556(4)	0.050(18)[a]		0.024^{+21}_{-15}
		1468.85(10)	0	0_1^+	0.3355(5)			0.32^{+7}_{-5}
1870.7	4_2^+	401.88(13)	1468.8	2_3^+	0.221(5)			[100(3)]
		455.29(13)	1415.6	4_1^+	0.120(4)	2.7^{+4a}_{-3}		[25(1)]
		558.39(11)	1312.4	2_2^+	0.356(7)			[31.1(6)]
		1253.16(12)	617.5	2_1^+	0.304(7)			[0.47(1)]
1871.1	0_4^+	402.50(16)	1468.8	2_3^+	0.098(7)			[100(7)]
		1253.56(12)	617.5	2_1^+	0.902(7)			[3.12(3)]
2064.6	3_1^+	648.83(11)	1415.6	4_1^+	0.124(5)	-1.20^{+20a}_{-15}	680(190)[a]	24^{+10}_{-6}
		752.19(11)	1312.4	2_2^+	0.456(11)	-2.75^{+23a}_{-17}		63^{+24}_{-14}
		1447.04(11)	617.5	2_1^+	0.419(11)	-1.70^{+10a}_{-12}		1.8^{+7}_{-4}
2081.9	4_3^+	613.15(13)	1468.8	2_3^+	0.089(5)		500(150)[a]	53^{+23}_{-12}
		666.16(11)	1415.6	4_1^+	0.497(14)	1.36(7)[a]		27^{+12}_{-7}
		769.43(11)	1312.4	2_2^+	0.364(13)			69^{+30}_{-16}
		1464.91(23)	617.5	2_1^+	0.050(13)			0.38^{+19}_{-13}
2121.6	2_4^+	688.26(11)	1433.4	0_3^+	0.125(6)		740(200)[a]	28^{+10}_{-6}
		809.49(21)	1312.4	2_2^+	0.0160(15)			$< 1.6^{+6}_{-4}$
		897.15(11)	1224.4	0_2^+	0.077(3)			4.6^{+17}_{-10}
		1504.04(11)	617.5	2_1^+	0.746(9)	1.36(7)		2.2^{+8}_{-5}
		2121.49(16)	0.0	0_1^+	0.036(5)			0.029^{+11}_{-7}
2156.2	2_5^+	285.1(3)	1871.1	0_4^+	0.00079(33)		310(35)[a]	34(15)
		687.35(11)	1468.8	2_3^+	0.0466(23)	$-2.3^{+19a}_{-\infty}$		21^{+5}_{-18}
		722.59(20)	1433.4	0_3^+	0.0024(3)			1.0(2)
		843.78(28)	1312.4	2_2^+	0.0050(6)			1.0(2)
		1538.67(11)	617.5	2_1^+	0.874(17)	0.085^{+25a}_{-22}		0.060^{+28}_{-40}
		2156.19(11)	0.0	0_1^+	0.071(17)			0.13(3)
2231.2	2_6^+	225.84(15)	2005.2	3_1^-	0.0091(4)		220(20)	
		360.1(2)	1871.1	0_4^+	0.00039(4)			7.5(15)
		762.47(11)	1468.8	2_3^+	0.0182(8)	-1.4^{+8}_{-34}		5.5^{+25}_{-30}
		797.96(11)	1433.4	0_3^+	0.0251(13)			9.0^{+8}_{-9}
		815.6(3)	1415.6	4_1^+	0.0096(4)			3.1(3)
		918.83(11)	1312.4	2_2^+	0.0239(11)	0.21^{+20}_{-13}		0.18^{+44}_{-16}
		1006.86(11)	1224.4	0_2^+	0.038(2)			4.3^{+5}_{-4}
		1613.71(11)	617.5	2_1^+	0.875(4)	-0.02^{+2}_{-3}		0.004^{+17}_{-4}
2403.2	3_2^+	531.89(6)[b]	1870.7	4_2^+	0.035(4)	-0.6^{+4}_{-25}	340^{+150}_{-80}	16^{+40}_{-15}
		934.28(12)	1468.8	2_3^+	0.277(17)	$-4.0(6)$[a]		27(9)
		987.39(12)	1415.6	4_1^+	0.234(15)	-0.025^{+27}_{-36}		0.012^{+58}_{-12}
		1090.95(16)	1312.4	2_2^+	0.236(20)	0.099^{+27}_{-36}		0.011(8)
		1785.85(16)	617.5	2_1^+	0.220(11)	-0.107^{+36}_{-43}		0.010^{+10}_{-7}
2711.3	4_6^+	555.0(3)	2156.3	2_5^+	0.059(8)		370^{+210}_{-100}	77(30)
		630.0(3)	2081.3	4_3^+	0.066(10)			46(18)
		1295.64(12)	1415.6	4_1^+	0.876(20)	$-0.08(6)$		0.11^{+21}_{-11}

[a] Value taken from Ref. [59].
[b] Value taken from Ref. [36]

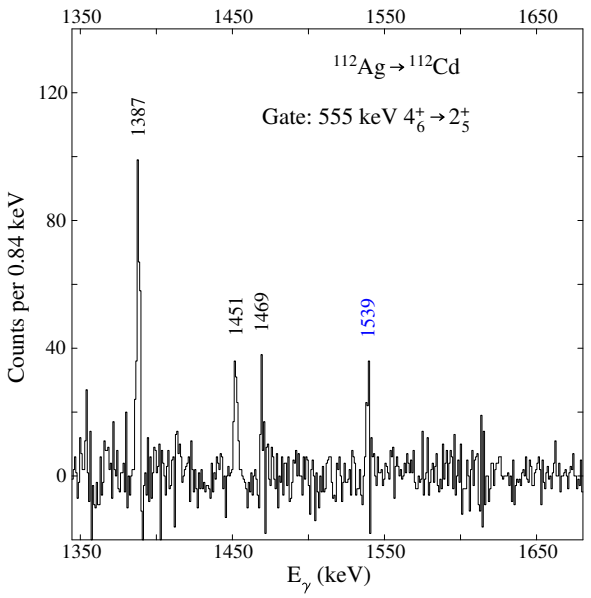

FIG. 12. Portion of the spectrum of γ rays in coincidence with the 555 keV $4_6^+ \rightarrow 2_5^+$ γ ray. The 1387, 1451, and 1469 keV γ rays arise from a 555 keV transition from the 3422 keV level to the 2867 keV 3^- state.

on $\pi(4p6h)$ excitations. This suggestion was made based, in part, on the observed parabolic trend in their excitation energies as shown in Fig. 1, and their preferred decay to the $\pi(2p4h)$ intruder excitations. This scenario might be expected to generate a configuration with a higher degree of deformation. In order to explore this possibility, beyond-mean-field calculations were performed.

Nuclear energy density functional methods, i.e., self-consistent mean-field and beyond-mean-field approaches, are, generally, based on the variational principle to solve the complex nuclear many-body problem. Therefore, the quality of the approximation will depend on the complexity of the nuclear wave functions that are contained in the variational space, and, obviously, on the reliability of the effective nuclear interaction used in the calculations. One of the most sophisticated variational methods of this kind is the so-called symmetry conserving configuration mixing method (SCCM) with Gogny (or Skyrme/Relativistic) interactions [60]. Some of the important aspects of this method are: 1) it is a microscopic approach; 2) it is parameter-free in the sense that the nuclear interaction is not designed and/or fitted to a specific region of the nuclear chart, and; 3) the nuclear states in the laboratory frame are obtained by mixing intrinsic states with well-defined deformations. Therefore, this method is an excellent theoretical tool to study nuclear aspects related to the shape of the nucleus such as vibrations and rotations, shape evolution, shape coexistence, and/or shape mixing.

The starting point of the SCCM is the definition of the nuclear states with angular momentum J through the ansatz (generator coordinate method, GCM) [61]:

$$|\Psi^{J\sigma}\rangle = \sum_{\vec{q}} f_{\vec{q}}^{J\sigma} |\Phi_{\vec{q}}^{J}\rangle \tag{4}$$

where $\sigma = 1, 2, ...$ labels the different states for a given J and $|\Phi_{\vec{q}}^{J}\rangle$ are the projected intrinsic states:

$$|\phi_{\vec{q}}^{J}\rangle = P^J P^N P^Z |\vec{q}\rangle. \tag{5}$$

In the above expression, P^J, P^N, and P^Z are the projectors onto good angular momentum, neutron number, and proton number, respectively [61]. Furthermore, the intrinsic states, $|\vec{q}\rangle$, have the structure of Hartree-Fock-Bogoliubov (HFB) states and are obtained by solving particle number variation after projection (PN-VAP) equations, imposing the constraints on the corresponding collective coordinates $\vec{q}$. Hence, we minimize the modified particle number projected energy [61]:

$$\begin{aligned} E'_{\vec{q}} = & \frac{\langle \vec{q}|\hat{H}P^N P^Z|\vec{q}\rangle}{\langle \vec{q}|P^N P^Z|\vec{q}\rangle} - \lambda_N \langle \vec{q}|\hat{N}|\vec{q}\rangle \\ & - \lambda_Z \langle \vec{q}|\hat{Z}|\vec{q}\rangle - \vec{\lambda}_{\vec{q}} \cdot \langle \vec{q}|\hat{\vec{Q}}|\vec{q}\rangle \end{aligned} \tag{6}$$

where the Lagrange multipliers λ_N, λ_Z, and $\vec{\lambda}_{\vec{q}}$ ensure that the intrinsic states fulfill the constraints in the neutron and proton numbers and in the collective coordinates, i.e., $\langle \vec{q}|\hat{N}|\vec{q}\rangle = N$, $\langle \vec{q}|\hat{Z}|\vec{q}\rangle = Z$, and $\langle \vec{q}|\hat{\vec{Q}}|\vec{q}\rangle = \vec{q}$, respectively. In the present study, a general quadrupole deformation is included, i.e., $\vec{q} = (q_{20}, q_{22})$, or equivalently, (β_2, γ). However, we do not allow for either parity (e.g., octupole degree of freedom) or time-reversal symmetry breaking. The first condition limits the study to positive-parity states only [62]. The second condition produces, in general, excitation energy spectra that are stretched compared with the experimental spectra because the ground-state energy is favored with respect to excited state energies by this implementation of the variational principle [63, 64]. Furthermore, the intrinsic wave functions are strictly quasiparticle vacua for their respective deformations which means that explicit quasiparticle excitations are not taken into account in the present approach and non-collective states cannot be described properly.

The last step to obtain the excitation energy spectrum, and other useful quantities such as the collective wave functions and transition probabilities, is the configuration (shape) mixing within the GCM framework (see Ref. [60] for details), requiring the solution for the coefficients of the linear combination given in Eq. 4. These coefficients are found by solving the Hill-Wheeler-Griffin (HWG) equations, one for each value of the angular momentum [61]:

$$\sum_{\vec{q}'} \left(\langle \phi_{\vec{q}}^{J}|\hat{H}|\phi_{\vec{q}'}^{J}\rangle - E^{J\sigma} \langle \phi_{\vec{q}}^{J}|\phi_{\vec{q}'}^{J}\rangle \right) f_{\vec{q}'}^{J\sigma} = 0 \tag{7}$$

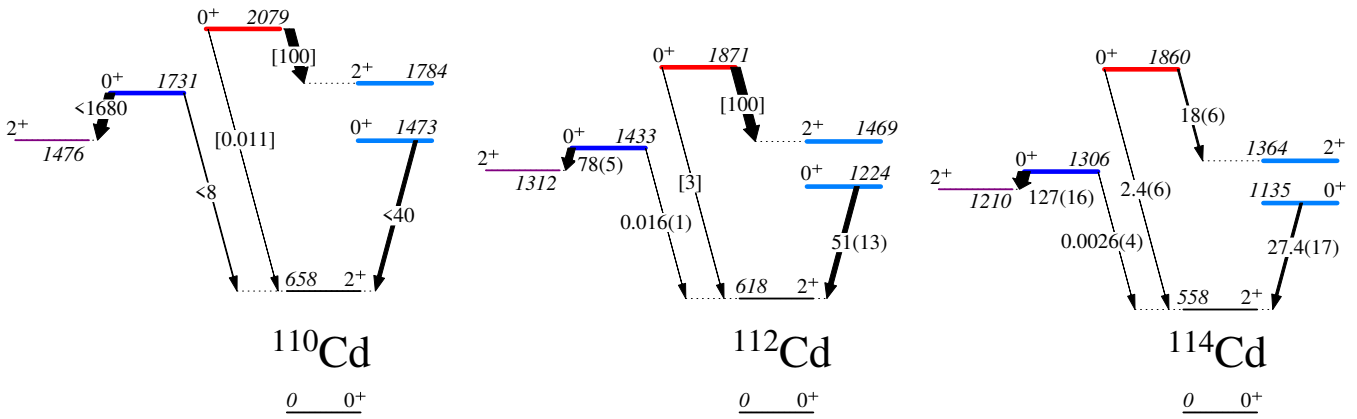

FIG. 13. Summary of the observed decays of the 0_2^+, 0_3^+, and 0_4^+ levels in ^{110,112,114}Cd. The widths of the arrows are proportional to the $B(E2)$ values, and the transitions are labeled with the absolute $B(E2)$ values in W.u. with uncertainties in parenthesis, or relative $B(E2)$ values in square brackets. The data show the enhanced decay of the 0_2^+ intruder band head to the 2_1^+ level, the enhanced decay of the 0_3^+ state to the 2_2^+ γ band head, and the preferred decay of the 0_4^+ level to the 2_3^+ intruder band member.

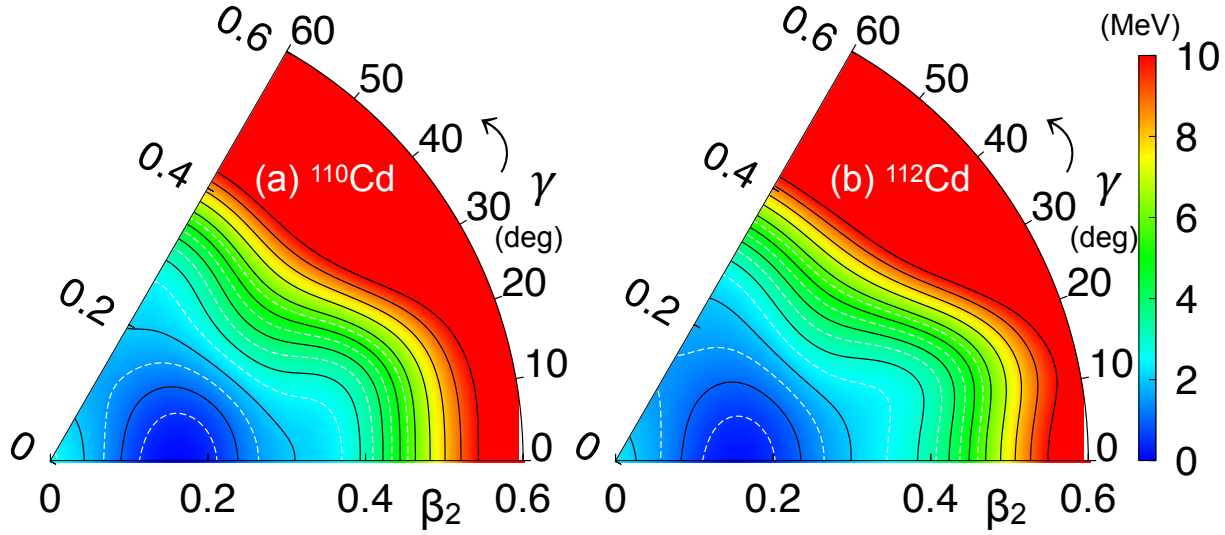

FIG. 14. PN-VAP energies in the (β_2, γ) plane for (a) ^{110}Cd and (b) ^{112}Cd calculated with the Gogny D1S interaction.

Once the above equations are solved, we obtain the energies ($E^{J\sigma}$), and the wave functions are used to compute electromagnetic properties ($B(E2)$, $Q_{\rm spec}$, etc.) and the collective wave functions. The latter are very useful to analyze the collective character of each individual state because they show the most relevant deformations needed to build those states. Moreover, states connected by strong $E2$ transitions normally show similar collective wave functions so the character of the bands can be described in more detail.

SCCM applications with the most widely used EDF (Skyrme, Gogny, Relativistic Lagrangians) could present ill-defined terms because of [65–69]: 1) using different interactions in the particle-hole (ph) and particle-particle (pp) channels; 2) neglecting exchange terms (particularly, Coulomb exchange); and, 3) the non-integer powers of the density contained in the functional. In the present calculations, both ph and pp channels come from the same underlying Gogny interaction and exchange and pairing terms are all included exactly (unlike Skyrme/Relativistic Lagrangians). Concerning the potential remaining problem, we choose a convenient prescription for the density-dependent term that is well-behaved within the present approach (see Refs. [70, 71] for more details). As a final remark, systematic and statistical errors are very hard to estimate in this kind of EDF calculation. The latter should be estimated by propagating the errors of the parameters of the interaction. However, this would require the repetition of the calculations a large number of times, which is not feasible

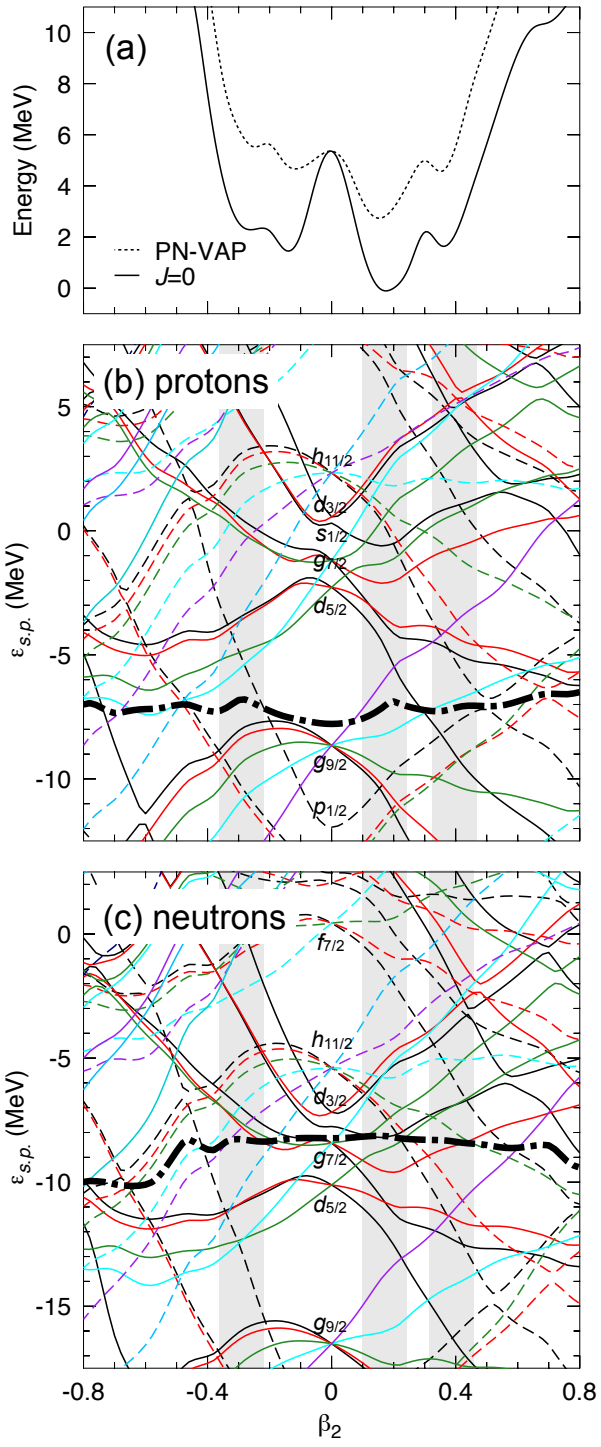

FIG. 15. (a) Potential energy surfaces computed within PN-VAP (dotted line) and angular momentum projection (continuous line) approximation, and, single-particle energies for (b) protons and (c) neutrons, as a function of the axial quadrupole deformation (thick dash-dotted lines represent the Fermi energies). Shaded areas mark the position of the minima in the PES. The calculations are performed with Gogny D1S interaction for ^{110}Cd.

from the computational point of view. The evaluation of the systematic error is also difficult because of several reasons. On the one hand, uncertainties in the excitation energies and transition probabilities associated with the convergence in the size of the working basis or the convergence of the HWG equations are normally negligible [72, 73], but a systematic study of such aspects requires, again, a large computational cost. On the other hand, SCCM methods do not provide the exact but approximate (variational) solutions. Thus, the role of the collective and non-collective degrees of freedom not included in these calculations is difficult to quantify with an error bar. Finally, the ability of the Gogny interaction itself to describe nuclear data cannot be easily estimated with a plain number. Recently, statistical tools such as Bayesian analyses have been proposed to give reliable estimations of the model errors [74–76]. However, such sophisticated techniques have not been applied in the present work and, therefore, we prefer to show the theoretical results without uncertainties.

A. SCCM with axial and triaxial quadrupole states

A first insight into the collective character of a nucleus is the analysis of the mean-field (or equivalently, the PN-VAP) energy as a function of the intrinsic deformation, (β_2, γ), i.e., the potential energy surface (PES). In Fig. 14 shows the PES for ^{110,112}Cd nuclei calculated with the Gogny D1S interaction. We observe that both isotopes show a distinct minimum at an axial prolate deformation $\beta_2 \approx 0.15$. Although this value is not far from the spherical point, it is sufficiently large enough to discard pure vibrational behavior of the ground state and the lowest excitations. Moreover, in both nuclei we observe PES shoulders at $(\beta_2, \gamma) \approx (0.4, 15°)$ and $(\beta_2, \gamma) \approx (0.1, 60°)$ that also play a role at higher excitation energies, as will be discussed below. Similar PESs are also obtained with Skyrme functionals [77].

The origin of the minima and the shoulders in the PES can be studied in terms of the underlying shell structure. To understand this behavior, we analyze in ^{110}Cd the PN-VAP and the angular momentum projected ($J = 0$) PES along the axial direction, i.e., $\gamma = 0°$ (prolate) and 60° (oblate). The latter can be expressed as negative values of β_2. In Fig. 15(a) we observe the energy gain obtained by the restoration of the rotational invariance of the system. We clearly see the absolute minimum at a prolate deformation, and three more minima, two in the oblate part and one at $\beta_2 \approx 0.4$. These minima are better defined in the angular momentum projected PES.

The occurrence of minima in the PES is related to the gaps in the proton and/or neutron single-particle energies (s.p.e.) that are crossed by the Fermi energy. These s.p.e.'s and Fermi energies are shown in Fig. 15(b)-(c) as a function of the axial quadrupole deformation (i.e., a Nilsson-like plot). The absolute minimum can be related to the proton energy gap crossed by the Fermi energy at

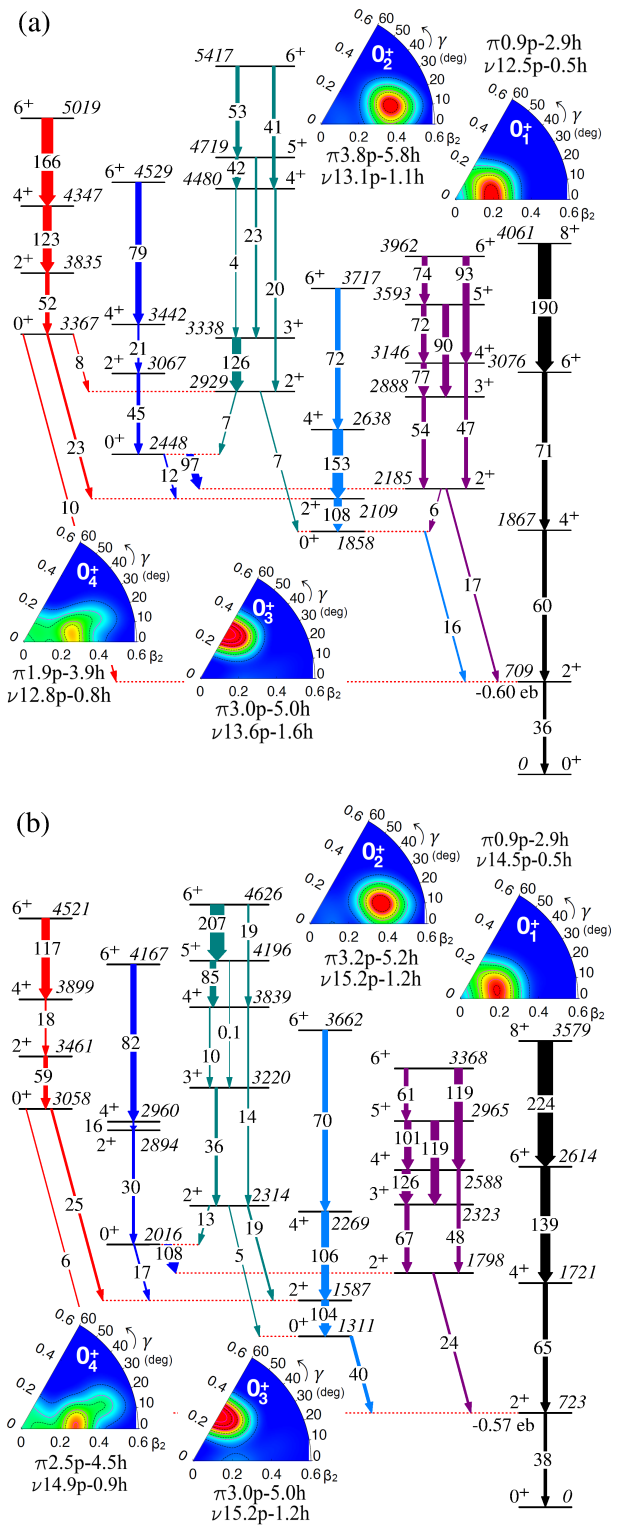

FIG. 16. Excitation energies (in keV) and $B(E2)$ values (in W.u.) computed with the SCCM method for (a) ^{110}Cd and (b) ^{112}Cd. The insets represent the collective wave functions in the (β_2, γ) plane for the band-heads and the particle-hole structure for those states.

$\beta_2 \approx 0.2$ which is produced by the rising of the $g_{9/2}$ and the lowering of the $d_{5/2}$ levels. The minima at oblate deformations are associated with the proton gap produced by levels coming from the $p_{1/2}$, $p_{3/2}$, $g_{7/2}$, $d_{5/2}$, $h_{11/2}$ and $g_{9/2}$ spherical orbitals. Finally, the secondary minimum at prolate deformation is related to the gap coming from $g_{9/2}$, $p_{1/2}$, $d_{5/2}$ and $h_{11/2}$ levels. The neutron level density around the Fermi energy is rather large in this range of deformations, and therefore neutrons are not playing a major role in the definition of the minima found in the PES. This fact is also the reason that the structures of the ^{110,112}Cd nuclei are similar.

The above analysis shows the complexity of the underlying single-particle structure of these isotopes. However, full SCCM calculations are required to obtain excitation energies and transition rates for comparisons with experimental data. Additionally, the collective behavior of the nucleus can be analyzed with the collective wave functions defined within the SCCM method [60], and the shell structure can be assessed by computing the occupation numbers of spherical orbitals for each individual nuclear state, taking into account all beyond-mean-field effects [78].

In Fig. 16, the excitation energies and $B(E2)$ values for the "in-band" transitions are plotted for ^{110,112}Cd. The states are ordered into sequences according to their $B(E2)$ values and collective wave functions. Some relevant interband transitions are also drawn. To shed light on the structure of the different bands, the collective wave functions of the lowest 0^+ states are also shown, where the colors (gray scale) indicate the weights of the different quadrupole deformations in each individual nuclear state, $|\Psi^{J\sigma}\rangle$. There is a great deal of similarity between the spectra of ^{110}Cd and ^{112}Cd, as might be expected from the similar PES shown in Fig. 14. For this region, neutrons are not playing a distinctive role in the structure of two adjacent isotopes due to the large level density around the neutron Fermi energy (see Fig. 15(c)). Therefore, we will focus our analysis on the nucleus ^{110}Cd.

In the low-energy part of the spectrum, four bands are obtained with 0^+ states as the band heads and possessing $\Delta J = 2$, and two bands with 2^+ states as the lowest states and $\Delta J = 1$. The collective wave functions of the band-heads are represented in Fig. 16, and a more detailed evolution of the deformation within a given band is shown in Fig. 17. It should be noted that the maxima of the collective wave functions are related to the minima of the PES shown, for example, in Fig. 15(a). Hence, the ground state has its maximum probability distribution at a prolate deformation ($\beta_2 \approx 0.20$), and this structure is also observed in the 2_1^+ and 4_1^+ states. For 6_1^+ and 8_1^+ states, a transition occurs towards triaxial deformations $(\beta_2, \gamma) \approx (0.4, 15°)$. These deformations are precisely the same as the relevant deformations for the states 0_2^+, 2_2^+ and 4_2^+ that belong to the first excited band. The band built on the 0_3^+ state (0_3^+, 2_5^+, 4_4^+ and 6_4^+ levels) displays an axial oblate deformed character with some shape mixing in the 4_4^+ state. Finally, the band with

the 0_4^+ band-head evolves from a shape-mixing of prolate configurations (including the spherical point), obtained for the 0_4^+ state, to well-deformed axial prolate states with $\beta_2 \approx 0.35$ for the 2_6^+, 4_6^+ and 6_5^+ levels.

The evolutions of the collective wave functions for the $\Delta J = 1$ bands built on the 2_3^+ and 2_4^+ states are more complicated than those for the 0^+ states (see Fig. 17). The 2_3^+ state displays a triaxial deformation at $(\beta_2, \gamma) \approx (0.25, 35°)$ and the 3_1^+ and 4_3^+ states are also of triaxial deformed character but with large shape mixing. The latter is connected with the less-mixed states, 5_1^+ and 6_3^+, through components in the wave function that led to a deformation around $(\beta_2, \gamma) \approx (0.40, 20°)$. This deformation is precisely that for the 2_4^+ band head. The even-J states of this band possess this deformation while the odd-J states have a smaller deformation. The 3_2^+ state has admixtures of both deformations connecting the states in the band.

Finally, we briefly discuss the particle-hole content of the $0_{1,2,3,4}^+$ states. These quantities are derived from the number of protons/neutrons occupying the orbitals defined by the spherical Hartree-Fock field (see Ref. [78] for details). Particles and holes are defined by taking a core made of the $0s$, $0p$, $0d1s$, $0f1p$ and $0g_{9/2}$ spherical orbitals as the reference. For a pure spherical HF configuration, ^{110}Cd has a $(0p2h)$ (protons) and $(12p0h)$ (neutrons) configuration. However, the onset of deformation destroys such a normal configuration not only in the ground state (with an average proton occupation giving a $(1p3h)$ state) but also in the rest of 0^+ excited states. In those cases, the average proton occupancies yield nearly $(4p6h)$, $(3p5h)$ and $(2p4h)$ configurations obtained for 0_2^+, 0_3^+, and 0_4^+ states, respectively (see Fig. 16). The most relevant proton and neutron spherical orbitals are the full gds+$h_{11/2}$ space, which would make a full shell model calculation computationally very demanding.

B. Comparison of $B(E2)$ values

Table III shows a comparison of the calculated $B(E2)$ values with the experimental results for ^{110}Cd. Generally, the in-band transitions are calculated to be larger than observed. For example, the ground state band has 36, 60, and 71 W.u. calculated *vs.* 27.0(8), 42(7), and 62(18) W.u. observed for the $2^+ \to 0^+$, $4^+ \to 2^+$, and $6^+ \to 4^+$ transitions, respectively. For the intruder band, the corresponding values are 108 and 153 W.u., calculated *vs.* 29(5) and 115(35) W.u. observed for the $2^+ \to 0^+$ and $4^+ \to 2^+$ transitions. The over-estimation of the predicted in-band values reflects the larger amount of deformation calculated for the states; this is also reflected in the predicted quadrupole moment of the 2_1^+ state of -0.60 eb compared to the experimentally determined value $-0.40(3)$ eb [58]. The same trend is observed for ^{112}Cd in Table IV; the ground state band is predicted as 38 and 65 W.u. *vs.* 30.3(2) and 63(8) W.u. observed for the $2^+ \to 0^+$ and $4^+ \to 2^+$ transitions (the value for the $6^+ \to 4^+$ transition is unknown), and the intruder band 104 W.u. predicted *vs.* 67^{+15}_{-11} W.u. observed for the $2^+ \to 0^+$ transition (no other absolute in-band rates are currently known). The experimentally deduced quadrupole moment of $= -0.38(3)$ eb [59] is smaller than the predicted value of -0.57 eb indicating that as in ^{110}Cd, the predicted deformation is slightly too large for ^{112}Cd.

TABLE III: Comparison of experimental and theoretical $B(E2)$ values in W.u. for observed transitions ^{110}Cd. The listing of two experimental values reflects two possible solutions for the mixing ratio δ. The quantities in parentheses are the uncertainties, and those in square brackets are relative $B(E2)$ values. The $B(E2)$ values are from the present work unless noted. The column with the heading BMF lists results of the present beyond-mean-field calculations, and the column under PDS-CM lists the results of Ref. [79] that use a $U(5)$ partial dynamical symmetry with configuration mixing.

Transition	$B(E2)$ (W.u.)		
	Experimental	BMF	PDS-CM
$2_1^+ \to 0_1^+$	27.0(8)[a]	36	27.0
$0_2^+ \to 2_1^+$	< 40[b]	16	14.12
$2_2^+ \to 2_1^+$	30(5)[a]	17	46.3
$2_2^+ \to 0_1^+$	1.35(20)[a]	2.7	0.0
$4_1^+ \to 2_1^+$	42(7)[a]	60	45.9
$0_3^+ \to 2_2^+$	< 1680[b]	97	56
$0_3^+ \to 2_1^+$	< 7.9[b]	0.33	0.25
$2_3^+ \to 2_2^+$	< 8[b]	0.96	0.96
$2_3^+ \to 0_2^+$	29(5)[b]	108	29
$2_3^+ \to 2_1^+$	0.32^{+10}_{-14},6.7^{+10}_{-9}[b]	3.9	0.0
$2_3^+ \to 0_1^+$	0.28(4)[b]	0.10	0.08
$0_4^+ \to 2_3^+$	[100(3)]	23	16.3
$0_4^+ \to 2_2^+$	[< 0.65]	1.7	1.2
$0_4^+ \to 2_1^+$	[0.011(1)]	9.7	31.8
$2_4^+ \to 2_1^+$	4.78(35),0.0023(9)	0.071	0.10
$3_1^+ \to 2_3^+$	< 5[b]	16	0.012
$3_1^+ \to 4_1^+$	2.9^{+9}_{-8},39(12)[b]	11	16.5
$3_1^+ \to 2_2^+$	22.7(69)[b]	54	41.1
$3_1^+ \to 2_1^+$	0.85(25)[b]	2.8	0.0
$4_2^+ \to 2_3^+$	< 0.5[b]	0.56	0.005
$4_2^+ \to 4_1^+$	11(5)[b]	12	27.5
$4_2^+ \to 2_2^+$	22(10)[b]	47	30.0
$4_2^+ \to 2_1^+$	0.14(6)[b]	0.29	0.0
$4_3^+ \to 2_3^+$	115(35)[b]	153	42.6
$4_3^+ \to 4_1^+$	1.8^{+10}_{-15}[b]	5.6	0.0
$4_3^+ \to 2_2^+$	1.2(4)[b]	1.4	0.0
$4_3^+ \to 2_1^+$	0.14(4)[b]	0.071	0.49
$2_5^+ \to 2_3^+$	< 5[b]	3.1	0.002
$2_5^+ \to 0_3^+$	24.2(22)[b]	45	22.3
$2_5^+ \to 4_1^+$	< 5[b]	0.060	0.19
$2_5^+ \to 2_2^+$	0.7^{+5}_{-6}[b]	3.6	0.12
$2_5^+ \to 0_2^+$	< 1.9[b]	0.61	0.2
$2_5^+ \to 2_1^+$	3.2(3),0.009^{+23}_{-8}[b]	1.2	0.0
$6_1^+ \to 4_3^+$	36(11)[b]	110	2.4
$6_1^+ \to 4_2^+$	< 5[b]	3.3	0.0
$6_1^+ \to 4_1^+$	62(18)[b]	71	55.3
$3_3^+ \to 2_3^+$	11(2),0.25^{+12}_{-15}	5.1	
$3_3^+ \to 2_2^+$	0.59(14)	6.6	
$3_3^+ \to 2_1^+$	0.032(10)	1.8	
$4_5^+ \to 2_4^+$	55(14)	20	
$4_5^+ \to 2_3^+$	1.3(4)	0.0029	

Continued on next page

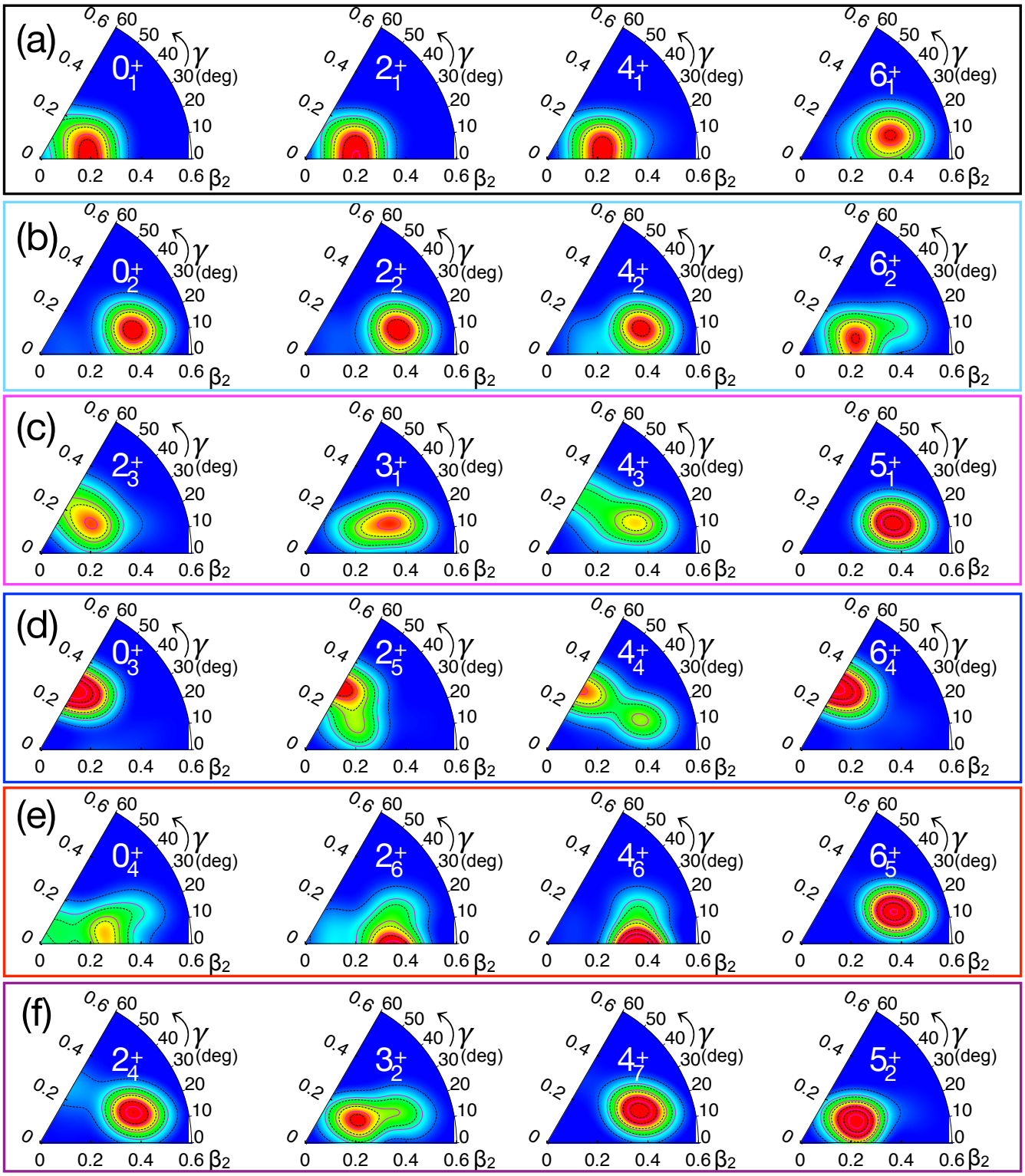

FIG. 17. Collective wave functions in the (β_2, γ) plane for the states grouped together as the different bands represented in Fig. 16(a) for ^{110}Cd. The panels coincide with the states associated to the a) ground state band, b) 0_2^+ intruder band, c) γ band, d) 0_3^+ band, e) 0_4^+ band, and f) intruder γ band.

Table III (continued)

Transition	$B(E2)$ (W.u.)		
	Experimental	BMF	PDS-CM
$4_5^+ \to 4_1^+$	$31(9), 0.09^{+56}_{-9}$	0.030	
$6_2^+ \to 6_1^+$	[< 164(36)]	12	
$6_2^+ \to 4_3^+$	[100(1)]	72	
$6_2^+ \to 4_1^+$	[1.29(1)]	19	
$5_1^+ \to 6_1^+$	$< 58^{+46}_{-39}$	21	
$5_1^+ \to 4_3^+$	$< 78^{+62}_{-52}$	11	
$5_1^+ \to 3_1^+$	140^{+110}_{-90}	90	
$5_1^+ \to 4_1^+$	$< 7^{+6}_{-5}$	1.4	
$5_2^+ \to 6_2^+$	[< 8400(600)]	11	
$5_2^+ \to 6_1^+$	[< 363(5)]	1.0	
$5_2^+ \to 4_3^+$	[< 107(2)]	0.84	
$5_2^+ \to 3_1^+$	[100(1)]	11	
$5_2^+ \to 4_1^+$	[< 2.63(3)]	1.3	
$6_3^+ \to 6_2^+$	[< 7500(160)]	6.0	
$6_3^+ \to 4_5^+$	[17.1(5)]	0.35	
$6_3^+ \to 6_1^+$	[< 115(1)]	16	
$6_3^+ \to 4_3^+$	[100(2)]	4.5	
$6_3^+ \to 4_1^+$	[0.32(1)]	0.079	
$6_4^+ \to 5_2^+$	[< 420(20)]	53	
$6_4^+ \to 5_1^+$	[< 200(5)]	13	
$6_4^+ \to 6_2^+$	[< 670(12)]	5.6	
$6_4^+ \to 4_5^+$	[100(2)]	41	
$6_4^+ \to 6_1^+$	$[33^{+24}_{-19}]$	2.9	
$6_4^+ \to 4_3^+$	[1.9(1)]	0.81	
$6_4^+ \to 4_2^+$	[17.7(3)]	0.024	
$6_4^+ \to 4_1^+$	[0.48(1)]	1.2×10^{-5}	

The decays from the band heads in both ^{110,112}Cd are generally well reproduced. The decay of the 0_2^+ state to the 2_1^+ state, in ^{110}Cd is predicted to be 16 W.u. with an observed upper limit of < 40 W.u., and in ^{112}Cd it is predicted to be 40 W.u., with 51(13) W.u. observed. The decays of the γ band heads are also in reasonable agreement, with predicted values of 17 and 24 W.u. and observed values of 30(5) and 40^{+7}_{-5} W.u. for ^{110}Cd and ^{112}Cd, respectively. (It should be noted that there exists considerable uncertainty on the $E2/M1$ mixing ratio δ for the $2_2^+ \to 2_1^+$ transition in ^{112}Cd. The evaluated magnitude adopted in the Nuclear Data Sheets [59] indicates an almost pure $E2$ transition, whereas the other possible solutions [36, 59] would result in a $B(E2)$ value of approximately 20 W.u., much closer to the theoretical result and in line with the other Cd isotopes.) The 0_3^+ states exhibit transitions to the γ band heads of < 1680 and 78(5) W.u. in ^{110}Cd and ^{112}Cd, respectively, and the theoretical values are 97 and 108 W.u. For the decays of the 0_3^+ states to the 2_1^+ levels, the corresponding values are < 7.9 and 0.016(1) W.u. observed, with 0.33 and 0.014 W.u. calculated. While the lifetimes for the 0_4^+ levels in ^{110,112}Cd are unknown, the relative $B(E2)$ values strongly favor their decays to the 2_3^+ intruder state by approximately 2 orders of magnitude (or more); this favored decay is also reflected in the calculations, although not nearly to the same degree.

[a] Value taken from Ref. [58].
[b] Value taken from Ref. [28].

As was discussed above, the predicted bands are mixed, and the mixing may be rather large for some spins where the locations of the unmixed levels are in proximity. For example, if we examine the collective wave function distributions for the 6_1^+ and 6_2^+ states in Fig. 17, we see that their characters appear to be interchanged; the collective wave function for the 6_1^+ state strongly resembles that for the 4_2^+, and that for the 6_2^+ more closely resembles the 4_1^+ state. To a lesser degree, we can see mixing in the wave functions for the 4_1^+ and 4_2^+ states as well. Thus, while the states are assigned as part of bands, the configurations may change as a function of spin, and in these cases, it is the presence of the large $B(E2)$ value that permits the assignment into band sequences. The results presented in Table III reflect this mixing; focusing on the 6_2^+ state, experimentally it has relative $B(E2)$ values for decay to the 6_1^+, 4_2^+ and 4_1^+ levels of $< 164(36)$ (where the upper limit results from the unknown $E2/M1$ mixing ratio), 100(1), and 1.29(1), respectively, and predicted to have absolute $B(E2)$ values of 12, 72, and 19 W.u., respectively. Thus, while the predicted wave function for the 6_2^+ state more closely resembles the lower spin members of the ground-state band, it has its largest $B(E2)$ value for decay to the 4^+ intruder-band member.

TABLE IV: Comparison of experimental results and theoretical calculations for ^{112}Cd. See caption to Table III.

Transition	$B(E2)$ (W.u.)	
	Experimental	BMF
$2_1^+ \to 0_1^+$	30.3(2)[a]	38
$0_2^+ \to 2_1^+$	51(13)[a]	40
$2_2^+ \to 2_1^+$	40^{+7}_{-5}	24
$2_2^+ \to 0_1^+$	0.64^{+12}_{-9}	1.7
$4_1^+ \to 2_1^+$	63(8)	65
$0_3^+ \to 2_2^+$	78(5)	108
$0_3^+ \to 2_1^+$	0.016(1)	0.014
$2_3^+ \to 0_2^+$	67^{+15}_{-11}	104
$2_3^+ \to 2_1^+$	0.024^{+21}_{-15}	8.8
$2_3^+ \to 0_1^+$	0.32^{+7}_{-5}	0.0009
$0_4^+ \to 2_3^+$	[100(3)]	25
$0_4^+ \to 2_2^+$	[< 9.5]	6.7
$0_4^+ \to 2_1^+$	[0.011(1)]	6.4
$2_4^+ \to 0_3^+$	28^{+10}_{-6}	30
$2_4^+ \to 2_2^+$	$< 1.6^{+6}_{-4}$	9.4
$2_4^+ \to 0_2^+$	4.6^{+17}_{-10}	5.3
$2_4^+ \to 2_1^+$	2.2^{+8}_{-5}	0.42
$2_4^+ \to 0_1^+$	0.029^{+11}_{-7}	0.068
$3_1^+ \to 4_1^+$	24^{+10}_{-6}	18
$3_1^+ \to 2_2^+$	63^{+24}_{-14}	67
$3_1^+ \to 2_1^+$	1.8^{+7}_{-4}	1.6
$4_2^+ \to 2_3^+$	[100(3)]	106
$4_2^+ \to 4_1^+$	[25(1)]	17
$4_2^+ \to 2_2^+$	[31.1(6)]	0.0061
$4_2^+ \to 2_1^+$	[0.47(1)]	4.5
$4_3^+ \to 2_3^+$	53^{+23}_{-12}	2.4
$4_3^+ \to 4_1^+$	27^{+12}_{-7}	20
$4_3^+ \to 2_2^+$	69^{+30}_{-16}	48
$4_3^+ \to 2_1^+$	0.38^{+19}_{-13}	0.062
$2_5^+ \to 0_4^+$	34(15)	59
$2_5^+ \to 2_3^+$	21^{+5}_{-18}	2.5

Continued on next page

Table IV (continued)

Transition	$B(E2)$ (W.u.) Experimental	BMF
$2_5^+ \to 0_3^+$	1.0(2)	0.0018
$2_5^+ \to 2_2^+$	1.0(2)	0.0017
$2_5^+ \to 2_1^+$	0.060^{+28}_{-40}	0.18
$2_5^+ \to 0_1^+$	0.13(3)	0.16
$6_1^+ \to 4_2^+$	[60(9)][a]	61
$6_1^+ \to 4_1^+$	[100.0(1)][a]	139
$3_2^+ \to 4_2^+$	16^{+40}_{-15}	10
$3_2^+ \to 2_3^+$	27(9)	0.87
$3_2^+ \to 4_1^+$	0.012^{+58}_{-12}	2.0
$3_2^+ \to 2_2^+$	0.011(8)	9.2
$3_2^+ \to 2_1^+$	0.010^{+10}_{-7}	1.6
$4_6^+ \to 2_5^+$	77(30)	18
$4_6^+ \to 4_3^+$	48(18)	1.9
$4_6^+ \to 4_1^+$	0.11^{+21}_{-11}	1.2×10^{-5}
$6_2^+ \to 6_1^+$	[23(4)][a]	29
$6_2^+ \to 4_2^+$	[100(3)][a]	6.5
$6_2^+ \to 4_1^+$	[7.2(3)][a]	1.1
$5_1^+ \to 4_3^+$	< 40	101
$5_1^+ \to 3_1^+$	< 250	119
$5_1^+ \to 4_2^+$	< 0.8	11
$5_1^+ \to 4_1^+$	< 0.1	3.7
$6_3^+ \to 4_3^+$	[100(4)][a]	119
$6_3^+ \to 4_1^+$	[2.1(2)][a]	1.1

Finally, for completeness in Table III, we present the results of recent interacting boson model calculations for ^{110}Cd by Leviatan *et al.* [79] that incorporated configuration mixing within a partial-dynamical symmetry approach (PDS-CM). These calculations utilized a term in the Hamiltonian that preserved the $U(5)$ symmetry for some parts of the spectrum, while it was broken for a subset of non-yrast states [79]. Unlike the present BMF calculations, the PDS-CM is a fit to the excitation energy spectrum and the transition $B(E2)$ values. As can be seen, the PDS-CM results reproduce the data very well, except those for the 0_4^+ state. A particular feature of these calculations is that they introduce a large anharmonicity, i.e., the two-phonon and three-phonon 0^+ states interchange their character, as do the three-phonon and four-phonon 2^+ states. Thus, the model predicts that the two-phonon 0^+ state should exist, but at higher excitation energy. The observed 0_4^+ state, as shown in Table III, does not match the properties predicted for the two-phonon excitation. A question, thus, arises "are there any excited 0^+ states, aside from the 0_2^+ state, that possess enhanced $B(E2)$ values for decay to the 2_1^+ level?" As shown in Fig. 7 in Ref. [49], no 0^+ state above the intruder band head in *any* of the Cd isotopes has enhanced $B(E2; 0^+ \to 2_1^+)$ values. While mixing may distribute the $E2$ strength amongst several levels, it would be expected that at least one state would possess moderate $E2$ strength; that no 0^+ state appears to show an enhancement in ^{110,112,114}Cd would suggest that the two-phonon 0^+ state does not exist. Similarly, for the 2^+ excitations, we may seek the state that still possess the three-phonon nature. As given in Ref. [79], it is the 2_6^+ level that is predicted to have this character, with dominant $E2$ decays of $B(E2; 2_6^+ \to 0_4^+) = 24.3$ W.u., $B(E2; 2_6^+ \to 4_1^+) = 15.7$ W.u., $B(E2; 2_6^+ \to 2_2^+) = 9.3$ W.u., and $B(E2; 2_6^+ \to 4_3^+) = 3.6$ W.u. The data presented in Fig. 8 of Ref. [49] again shows that no excited state appears to resemble this decay pattern. In fact, of the $^{110-116}$Cd isotopes, the only observed $2^+ \to 4_1^+$ decay is in the present work for the 2231 keV 2_6^+ state in ^{112}Cd, yielding $B(E2; 2_6^+ \to 4_1^+) = 3.1(3)$ W.u., and also a moderate value of $B(E2; 2_6^+ \to 0_4^+) = 7.5(15)$ W.u., but with a very small $B(E2; 2_6^+ \to 2_2^+) = 0.18^{+44}_{-16}$ W.u. This would also suggest that the three-phonon 2^+ state does not exist.

IV. CONCLUSIONS

Detailed γ-ray spectroscopy following the β decays of ^{110}Ag and ^{112}Ag/^{112}In have revealed the presence of weak decay branches from nonyrast states. Combined with lifetimes from $(n, n'\gamma)$ reaction measurements, the absolute $B(E2)$ values indicate collective structures built on the 0_3^+ and 0_4^+ levels, and candidates for γ bands built on the 0_2^+ intruder bands. These results are interpreted with the aid of beyond-mean-field calculations that suggest that the 0^+ states in ^{110,112}Cd represent examples of multiple shape coexisting structures. This new suggestion provides an alternative view of the structure of the Cd isotopes, long believed to be prime examples of nearly harmonic vibrational motion.

This interpretation needs rigorous testing, perhaps best and most directly performed with detailed Coulomb excitation studies designed to permit the extraction of the shape invariant quantities $\langle Q^2 \rangle$ and $\langle \cos 3\delta \rangle$ values. Further, additional highly sensitive β-decay studies, or other techniques, that would enable the observation of additional weak decay branches from other nonyrast levels are clearly needed.

ACKNOWLEDGMENTS

The assistance of Drs. F. Corminboeuf and L. Genilloud in the collection of the $(n, n'\gamma)$ data is gratefully acknowledged, as are discussions with M. Zielińska and A. Gezerlis. This work was supported in part by the Natural Sciences and Engineering Research Council (Canada), TRIUMF through the National Research Council (Canada), by the U.S. National Science Foundation under Grant No. PHY-1913028. T.R.R. acknowledges computing time at GSI-Darmstadt and support from Spanish MINECO under FIS-2014-53434-P.

[a] Value taken from Ref. [59].

[1] P.E. Garrett, J. Phys. G: Nucl. Part. Phys. **43** 084002 (2016).

[2] K. Heyde and J.L. Wood, Rev. Mod. Phys. **83**, 1467 (2011).

[3] R. Middleton, J.D. Garrett, and H.T. Fortune, Phys. Lett. **B39**, 339 (1972).

[4] E. Ideguchi, D.G. Sarantites, W. Reviol, A.V. Afanasjev, M. Devlin, C. Baktash, R.V.F. Janssens, D. Rudolph, A. Axelsson, M.P. Carpenter, A. Galindo-Uribarri, D.R. LaFosse, T. Lauritsen, F. Lerma, C.J. Lister, P. Reiter, D. Seweryniak, M. Weiszflog, and J.N. Wilson. Phys. Rev. Lett. **87**, 222501 (2001).

[5] K. Hadyńska-Klęk, P.J. Napiorkowski, M. Zielińska, J. Srebrny, A. Maj, F. Azaiez, J.J. Valiente Dobón, M. Kicińska-Habior, F. Nowacki, H. Naïdja *et al.*, Phys. Rev. Lett.**117**, 062501 (2016).

[6] K. Hadyńska-Klęk, P.J. Napiorkowski, M. Zielińska, J. Srebrny, A. Maj, F. Azaiez, J.J. Valiente Dobón, M. Kicińska-Habior, F. Nowacki, H. Naïdja *et al.*, Phys. Rev. C **97**, 024326(2018).

[7] C. De Coster, B. Decroix, and K. Heyde, Phys. Rev. C **61**, 067306 (2000).

[8] A.N. Andreyev, M. Huyse, P. Van Duppen, L. Weissman, D. Ackermann, J. Gerl, F.P. Hessberger, S. Hofmann, A. Kleinböhl, G. Münzenberg, S. Reshitko, C. Schlegel, H. Schaffner, P. Cagarda, M. Matos, S. Saro, A. Keenan, C. Moore, C.D. O'Leary, R.D. Page, M. Taylor, H. Kettunen, M. Leino, A. Lavrentiev, R. Wyss, and K. Heyde, Nature (London) **405**, 430 (2000).

[9] P.E. Garrett, T.R. Rodriguez, A.D.Varela, K.L. Green, J. Bangay, A. Finlay, R.A.E. Austin, G.C. Ball, D.S. Bandyopadhyay, V. Bildstein, S. Colosimo, D.S. Cross, G.A. Demand, P. Finlay, A.B. Garnsworthy, G.F. Grinyer, G. Hackman, B. Jigmeddorj, J. Jolie, W.D. Kulp, K.G. Leach, A.C. Morton, J.N. Orce, C.J. Pearson, A.A. Phillips, A.J. Radich, E.T. Rand, M.A. Schumaker, C.E. Svensson, C. Sumithrarachchi, S. Triambak, N. Warr, J. Wong, J.L. Wood, and S.W. Yates, Phys. Rev. Lett. **123**, 142502 (2019).

[10] L.K. Peker and M.E. Voichansky, Izv. Akad. Nauk SSSR Ser Fiz. **32**, 892 (1968).

[11] G. Gneuss and W. Greiner, Nucl. Phys. **A171**, 449 (1971).

[12] R. Meyer and L. Peker, Z. Phys. **A283**, 379 (1977).

[13] H.W. Fielding, R.E. Anderson, C.D. Zafiratos, D.A. Lind, F.E. Cecil, H.H. Wieman, and W.P. Alford, Nucl. Phys. **A281**, 389 (1977).

[14] J. Kumpulainen, R. Julin, J. Kantele, A. Passoja, W.H. Trzaska, E. Verho, and J. Vaaramaki, Z. Phys. **A335**, 109 (1990).

[15] J. Kumpulainen, R. Julin, J. Kantele, A. Passoja, W.H. Trzaska, E. Verho, J. Vaaramaki, D. Cutoiu, and M. Ivascu, Phys. Rev. C **45**, 640 (1992).

[16] M. Délèze, S. Drissi, J. Kern, P.A. Tercier, J.-P. Vorlet, J. Rikovska, T. Otsuka, S. Judge, and A. Williams, Nucl. Phys. **A551**, 269 (1993).

[17] M. Pignanelli, N. Blasi, S. Micheletti, R. de Leo, M.A. Hofstee, J.M. Schippers, S.Y. van der Werf, and M.N. Harakeh, Nucl. Phys. **A519**, 567 (1990).

[18] M. Pignanelli, N. Blasi, S. Micheletti, R. de Leo, L. LaGamba, R. Perrino, J.A. Bordewijk, M.A. Hofstee, J.M. Schippers, S.Y. van der Werf, J. Wesseling, and M.N. Harakeh, Nucl. Phys. **A540**, 27 (1992).

[19] R. de Leo, N. Blasi, S. Micheletti, M. Pignanelli, W.T.A. Borghols, J.M. Schippers, S.Y. van der Werf, G. Maino, and M.N. Harakeh, Nucl. Phys. **A504**, 109 (1989).

[20] A. Gade, J. Jolie, and P. von Brentano, Phys. Rev. C **65**, 041305(R) (2002).

[21] A. Gade, A. Fitzler, C. Fransen, J. Jolie, S. Kasemann, H. Klein, A. Linnemann, V. Werner, P. von Brentano, Phys. Rev. C **66**, 034311 (2002).

[22] J. Kern, A. Bruder, S. Drissi, V.A. Ionescu, and D. Kusnezov, Nucl. Phys. **A512**, 1 (1990).

[23] N. Blasi, S. Micheletti, M. Pignanelli, R. de Leo, R. Hertenberger, M. Bisemberger, D. Hofer, H. Kader, P. Schiemenz, and G. Graw, Nucl. Phys. **A536**, 1 (1992).

[24] R.L. Auble, D.J. Horen, F.E. Bertrand, and J.B. Ball, Phys. Rev. C **6**, 2223 (1972).

[25] M. Bertschy, S. Drissi, P.E. Garrett, J. Jolie, J. Kern, S.J. Mannanal, J.-P. Vorlet, N. Warr, and J. Suhonen, Phys. Rev. **C51**, 103 (1995).

[26] F. Corminboeuf, T. B. Brown, L. Genilloud, C. D. Hannant, J. Jolie, J. Kern, N. Warr, and S. W. Yates, Phys. Rev. Lett. **84**, 4060 (2000).

[27] F. Corminboeuf, T. B. Brown, L. Genilloud, C. D. Hannant, J. Jolie, J. Kern, N. Warr, and S. W. Yates, Phys. Rev. C **63**, 014305 (2000).

[28] P.E. Garrett, J. Bangay, A. Diaz Varela, G.C. Ball, D.S. Cross, G.A. Demand, P. Finlay, A.B. Garnsworthy, K.L. Green, G. Hackman, C.D. Hannant, B. Jigmeddorj, J. Jolie, W.D. Kulp, K.G. Leach, J.N. Orce, A.A. Phillips, A.J. Radich, E.T. Rand, M.A. Schumaker, C.E. Svensson, C. Sumithrarachchi, S. Triambak, N. Warr, J. Wong, J.L. Wood, and S.W.Yates, Phys. Rev. C **86**, 044304 (2012).

[29] M. Koike, Nucl. Phys. **A98**, 209 (1967).

[30] M. Koike, I. Nonaka, J. Kokame, H. Kamitsubo, Y. Awaya, T. Wada, and H. Nakamura, Nucl. Phys. **A125**, 161 (1969).

[31] N. Blasi, S. Micheletti, M. Pignanelli, R. de Leo, R. Hertenberger, F.J. Eckle, H. Kader, P. Schiemenz, and G. Graw, Nucl. Phys. **A551**, 251 (1990).

[32] R. Hertenberger, G. Eckle, F.J. Eckle, G. Graw, D. Hofer, H. Kader, P. Schiemenz, Gh. Cata-Danil, C. Hategan, N. Fujiwara, K. Hosono, M. Kondo, N. Matsuoka, T. Noro, T. Saito, S. Kato, S. Matsuki, N. Blasi, S. Micheletti, R. de Leo, Nucl. Phys. **A574**, 414 (1994).

[33] M. Délèze, S. Drissi, J. Jolie, J. Kern, and J.-P. Vorlet, Nucl. Phys. **A554**, 1 (1993).

[34] H. Lehmann, P.E. Garrett, J. Jolie, C.A. McGrath, Minfang Yeh, and S.W. Yates, Phys. Lett. B **387**, 259 (1996).

[35] S. Drissi, P.A. Tercier, H.G. Börner, M. Délèze, F. Hoyler, S. Judge, J. Kern, S.J. Mannanal, G. Mouze, K. Schreckenbach, J-.P. Vorlet, N. Warr, A. Williams, and C. Ythier, Nucl. Phys. **A614**, 137 (1997).

[36] P.E. Garrett, H. Lehmann, J. Jolie, C.A. McGrath, M. Yeh, W. Younes, and S.W. Yates, Phys. Rev. C **64**, 024316 (2001).

[37] P.E. Garrett, K.L. Green, H. Lehmann, J. Jolie, C.A. McGrath, M. Yeh, and S.W. Yates, Phys. Rev. **75**, 054310 (2007).

[38] K.L. Green, P.E. Garrett, R.A.E. Austin, G.C. Ball, D.S.

Bandyopadhyay, S. Colosimo, D. Cross, G.A. Demand, G.F. Grinyer, G. Hackman, W.D. Kulp, K.G. Leach, A.C. Morton, C.J. Pearson, A.A. Phillips, M.A. Schumaker, C.E. Svensson, J. Wong, J.L. Wood, and S.W. Yates, Phys. Rev. C **80**, 032502(R) (2009).

[39] D.S. Jamieson, P.E. Garrett, V. Bildstein, G.A. Demand, P. Finlay, K.L. Green, K.G. Leach, A.A. Phillips, C.S. Sumithrarachchi, C.E. Svensson, S. Triambak, G.C. Ball, T. Faestermann, R. Hertenberger, and H.-F. Wirth. Phys. Rev. C **90**, 054312 (2014).

[40] D.S. Jamieson, P.E. Garrett, G.C. Ball, G.A. Demand, T. Faestermann, P. Finlay, K.L. Green, R. Hertenberger, K.G. Leach, A.A. Phillips, C.S. Sumithrarachchi, S. Triambak, and H.-F. Wirth, Phys. Rev. C **98**, 044309 (2018).

[41] K. Schreckenbach, A. Mheemeed, G. Barreau, T. von Egidy, H.R. Faust, H.G. Börner, R. Brissot, M.L. Stelts, K. Heyde, P. van Isacker, M. Waroquier, and G. Wenes, Phys. Lett. B **110**, 364 (1982).

[42] A. Mheemeed, K. Schreckenbach, G. Barreau, H.R. Faust, H.G. Börner, R. Brissot, P. Hungerford, H.H. Schmidt, H.J. Scheerer, T. von Egidy, K. Heyde, J.L. Wood, P. Van Isacker, M. Waroquier, G. Wenes, and M.L. Stelts, Nucl. Phys. **A412**, 113 (1984).

[43] C. Fahlander, A. Bäcklin, L. Hasselgren, A. Kavka, V. Mittal, L.E. Svensson, B. Varnestig, D. Cline, B. Kotlinski, H. Grein, E. Grosse, R. Kulessa, C. Michel, W. Spreng, H.J. Wollersheim, and J. Stachel, Nucl. Phys. **A485**, 318 (1988).

[44] R.F. Casten, J. Jolie, H.G. Börner, D.S. Brenner, N.V. Zamfir, W.-T. Chou, and A. Aprahamian, Phys. Lett. B **297**, 19 (1992).

[45] D. Bandyopadhyay, S.R. Lesher, C. Fransen, N. Boukharouba, P.E. Garrett, K.L. Green, M.T. McEllistrem, and S.W. Yates, Phys. Rev. C **76**, 054308 (2007).

[46] M. Kadi, N. Warr, P.E. Garrett, J. Jolie, and S.W. Yates, Phys. Rev. C **68**, 031306(R) (2003).

[47] Y. Wang, P. Dendooven, J. Huikari, A. Jokinen, V.S. Kolhinen, G. Lhersonneau, A. Nieminen, S. Nummela, H. Penttilä, K. Peräjärvi, S. Rinta-Antila, J. Szerypo, J.C. Wang, and J. Äystö, Phys. Rev. C **64**, 054315 (2001).

[48] J.C. Batchelder, J.L. Wood, P.E. Garrett, K.L. Green, K.P. Rykaczewski, J.-C. Bilheux, C.R. Bingham, H.K. Carter, D. Fong, R. Grzywacz, J.H. Hamilton, D.J. Hartley, J.K. Hwang, W. Krolas, W.D. Kulp, Y. Larochelle, A. Piechaczek, A.V. Ramayya, E.H. Spejewski, D.W. Stracener, M.N. Tantawy, J.A. Winger, and E.F. Zganjar, Phys. Rev. C **80**, 054318 (2009).

[49] P.E. Garrett, K.L. Green, and J.L. Wood, Phys. Rev. C **78**, 044307 (2008).

[50] P.E. Garrett, A.J. Radich, J.M. Allmond, C. Andreoiu, G.C. Ball, P.C. Bender, L. Bianco, V. Bildstein, H. Bidaman, R. Braid, C. Burbadge, S. Chagnon-Lessard, D.S. Cross, G. Deng, G.A Demand, A. Diaz Varela, M.R. Dunlop, R. Dunlop, P. Finlay, A.B. Garnsworthy, G.F. Grinyer, G. Hackman, B. Hadinia, S. Ilyushkin, B. Jigmeddorj, D. Kisliuk, K. Kuhn, A.T. Laffoley, K.G. Leach, A.D. MacLean, J. Michetti-Wilson, D. Miller, W. Moore, B. Olaizola, J.N. Orce, C.J. Pearson, J.L. Pore, M.M. Rajabali, E.T. Rand, F. Sarazin, J.K. Smith, K. Starosta, C.S. Sumithrarachchi, C.E. Svensson, S. Triambak, J. Turko, Z.M. Wang, J.L. Wood, J. Wong, S.J. Williams, S.W. Yates, E.F. Zganjar, J. Phys. G. Conf. Ser. **639**, 012006 (2015).

[51] A.B. Garnsworthy and P.E. Garrett, Hyper. Int. **225**, 121 (2014).

[52] J. Dilling, R. Krücken, and G. Ball, Hyper. Int. **225**, 1 (2014).

[53] J. Lassen, P. Bricault, M. Dombsky, J.P. Lavoie, C. Geppert, K. Wendt, Hyper. Int. **162**, 69 (2005).

[54] W.D. Kulp, J.L. Wood, J.M. Allmond, J. Eimer, D. Furse, K.S. Krane, J. Loats, P. Schmelzenbach, C.J. Stapels, R.-M. Larimer, E.B. Norman, and A. Piechaczek, Phys. Rev. C **76**, 034319 (2007).

[55] A.J. Radich, P.E. Garrett, J.M. Allmond, C. Andreoiu, G.C. Ball, L.Bianco, V. Bildstein, S. Chagnon-Lessard, D.S. Cross, A. Diaz Varela, R. Dunlop, P. Finlay, A.B. Garnsworthy, G. Hackman, B. Hadinia, B. Jigmeddorj, A.T. Laffoley,K.G. Leach, J. Michetti-Wilson, J.N. Orce, M.M. Rajabali, E. Rand, K. Starosta, C.S. Sumithrarachchi, C.E. Svensson, S. Triambak, Z. M. Wang, J.L. Wood, J. Wong, S.J. Williams, and S.W. Yates, Proc. of the 2'nd Conf. on Adv. Radioactive Isotope Science, ARIS2014, Tokyo, Japan, June 2014, Jap. Phys. Soc. Conf. Proc. **6** 030015 (2015).

[56] T. Belgya, G. Molnár, and S. W. Yates, Nucl. Phys. **A607**, 43 (1996).

[57] B. Jigmeddorj, P.E. Garrett, A. Diaz Varela, J.C. Bangay, G.A. Demand, K.L. Green, K.G. Leach, E.T. Rand, C. Sumithrarachchi, C.E. Svensson, S. Triambak, J. Wong, G.C. Ball, A.B. Garnsworthy, G. Hackman, D.S. Cross, W.D. Kulp, J.L. Wood, and S.W. Yates, E. Phys. J. A **52**, 36 (2016).

[58] G. Gurdal and F.G. Kondev, Nucl. Data Sheets **113**, 1315 (2012).

[59] S. Lalkovski and F.G. Kondev, Nucl. Data Sheets **124**, 157 (2015).

[60] T.R. Rodríguez, and J.L. Egido, Phys. Rev. C **81**, 064323 (2010).

[61] P. Ring, and P. Schuck, *The nuclear many body problem*, Springer-Verlag, Berlin, 1980.

[62] R.N. Bernard, L.M. Robledo, and T.R. Rodríguez, Phys. Rev. C **93**, 061302(R) (2016).

[63] M. Borrajo, T.R. Rodríguez, and J.L. Egido, Phys. Lett. **B746**, 341 (2015).

[64] J.L. Egido, M. Borrajo, T.R. Rodríguez, Phys. Rev. Lett. **116**, 052502 (2016).

[65] M. Anguiano, J.L. Egido, and L.M. Robledo, Nucl. Phys. **A696**, 467 (2001).

[66] J. Dobaczewski, M.V. Stoitsov, W. Nazarewicz, and P.-G. Reinhard, Phys. Rev. C **76**, 054315 (2007).

[67] D. Lacroix, T. Duguet, and M. Bender, Phys. Rev. C **79** 044318 (2009).

[68] M. Bender, T. Duguet, and D. Lacroix, Phys. Rev. C **79** 044319 (2009).

[69] T. Duguet, M. Bender, K. Bennaceur, D. Lacroix, and T. Lesinski, Phys. Rev. C **79** 044320 (2009).

[70] N.L. Vaquero, J.L. Egido, T.R. Rodríguez, Phys. Rev. C **88**, 064311 (2013).

[71] J.L. Egido, Phys. Scr. **91**, 073003 (2016).

[72] A. Arzhanov, T.R. Rodríguez, G. Martínez-Pinedo, Phys. Rev. C **94**, 054319 (2016).

[73] L.M. Robledo, T.R. Rodríguez, R.R. Rodríguez-Guzmán, J. Phys. G: Nucl. Part. Phys. **46**, 013001 (2019).

[74] J. Dobaczewski, W. Nazarewicz, and P. Reinhard, J. Phys. G: Nucl. Part. Phys. **41**, 074001 (2014).

[75] J.D. McDonnell, N. Schunck, D. Higdon, J. Sarich, S.M. Wild, and W. Nazarewicz, Phys. Rev. Lett. **114**, 122501

(2015).
[76] L. Neufcourt, Y. Cao, W. Nazarewicz, and F. Viens, Phys. Rev. C **98**, 034318 (2018).
[77] K. Nomura and J. Jolie, Phys. Rev. C **98**, 024303 (2018).
[78] T.R. Rodríguez, A. Poves, and F. Nowacki, Phys. Rev. C **93**, 054316 (2016).
[79] A. Leviatan, N. Gavrielov, J.E. García-Ramos, and P. Van Isacker, Phys. Rev. C **98**, 031302(R) (2018).